One vanishing minor in the neutrino mass matrix using trimaximal mixing

Iffat Ara Mazumder* and Rupak Dutta†
National Institute of Technology Silchar, Silchar 788010, India

(Received 13 January 2023; accepted 31 May 2023; published 15 June 2023)

We investigate the implications of one vanishing minor in the neutrino mass matrix using trimaximal mixing matrix. In this context, we analyze all six patterns of one vanishing minor zero in the neutrino mass matrix and present correlations of the neutrino oscillation parameters. All the six patterns are found to be phenomenologically viable with the present neutrino oscillation data. We also predict the values of effective Majorana mass, the effective electron antineutrino mass, and the total neutrino mass for all the patterns. The value obtained for the effective neutrino mass is within the reach future neutrinoless double β decay experiments. We also propose a flavor model where such patterns can be generated within the seesaw model.

DOI: 10.1103/PhysRevD.107.115023

I. INTRODUCTION

Evidence of neutrino oscillations observed in multitude of experiments confirms that neutrinos mix with each other and have nonzero mass [1]. Neutrino oscillation phenomena can be parametrized in terms of six independent parameters, namely three mixing angles $(\theta_{13}, \theta_{12}, \theta_{23})$, one Dirac CP violating phase (δ_{CP}), and two mass squared differences $(\Delta m^2_{21}, \Delta m^2_{31})$. Although we have very precise values of the mixing angles and the absolute value of the mass squared differences, there are still some unknowns such as the octant of θ_{23}, δ_{CP} and the sign of Δm^2_{31}. There are two possible mass ordering of the neutrino mass spectrum: normal mass ordering (NO) $m_1 < m_2 \ll m_3$ and inverted mass ordering (IO) $m_3 \ll m_1 < m_2$ depending on the sign of Δm^2_{31}.

Neutrino oscillation experiments are sensitive only to the mass squared differences. They cannot provide any information regarding the absolute mass scale of neutrinos which is one of the most sought after questions in particle physics today. Knowledge of the absolute mass scale of neutrinos is of great importance not only in particle physics but also in understanding the large scale structure of our universe. Neutrinos possess very tiny mass and unlike all other fermions in the Standard Model (SM), they do not seem to get their mass through Higgs mechanism. Hence, it may, in principle, help shape our understanding of the origin of particle mass which is still one of the most fundamental questions of particle physics. Unlike all other fermions in the SM, we observe only left handed neutrinos and right handed antineutrinos. We have not found any right handed neutrino and left handed antineutrino so far in experiments. This brings us to the next relevant question whether neutrino is a Dirac particle or a Majorana particle. Neutrino interactions could violate CP as well which will be crucial in explaining the matter antimatter asymmetry in the universe. Moreover, there could be additional sterile neutrinos.

There are several experimental efforts to find the absolute mass of the neutrino. The β decay experiment performed at KATRIN can, in principle, measure the effective electron antineutrino mass by studying the endpoint region of the β decay spectrum. This is completely model independent determination, i.e., it depends neither on any cosmological models nor on the nature of neutrinos. At present, the improved upper bound on the effective electron antineutrino mass is reported to be $m_\nu < 0.8$ eV at 90% confidence level. The KATRIN experiment will continue to take data over the next several years and it is expected that the mass sensitivity will reach up to 0.2 eV. Future experiments like Project 8 [2], designed to measure the absolute mass scale of the neutrino, hopes to reach a goal of 40 meV/c^2 neutrino mass sensitivity. Indirectly, one can have information on neutrino mass from cosmological observations. These cosmological observations are sensitive to the total neutrino mass and to the number of neutrino species. There are several results related to the total neutrino mass coming from various cosmological observations. Most of these indirect methods put a limit on the total neutrino mass to be less than 0.2 eV. These results are, however, model dependent. They rely heavily on several cosmological assumptions. Current upper bound on the total neutrino mass is reported by the Planck satellite to be $\sum m_i <$ 0.12 eV at 95% confidence level combining BAO data with CMB data [3]. If KATRIN's mass sensitivity reach up to 0.2 eV in future, it can put severe constraint on several

*iffat_rs@phy.nits.ac.in
†rupak@phy.nits.ac.in

Published by the American Physical Society under the terms of the Creative Commons Attribution 4.0 International license. Further distribution of this work must maintain attribution to the author(s) and the published article's title, journal citation, and DOI. Funded by SCOAP³.

cosmological models. Rare double β decay process with two anti neutrinos in the final state is allowed in the SM. In general double beta decay processes are powerful probes of beyond the SM physics. More specifically, if one observes neutrinoless double β decay in experiments, it would confirm that neutrinos are Majorana in nature. One can determine the effective Majorana mass M_{ee} by studying neutrinoless double beta decay. There exists several limits on the value of M_{ee} using different isotopes. At present, the best limits are reported to be $m_{ee} < (0.079\text{–}0.18)$ eV, $m_{ee} < (0.075\text{–}0.35)$ eV and $m_{ee} < (0.061\text{–}0.165)$ eV [4–7], respectively.

There are several theoretical efforts in explaining the origin of neutrino mass. The most natural way to understand neutrino mass is through seesaw mechanism. The neutrino mass matrix in the framework of type-I seesaw mechanism is given by $M_\nu = -M_D M_R^{-1} M_D^T$, where M_D is the Dirac neutrino mass matrix and M_R is the Majorana mass matrix of the right-handed neutrinos. Phenomenology of the Majorana neutrino mass matrix has been studied extensively assuming zero textures of the neutrino mass matrix which may be realized from the zeros in M_D or M_R. In literature, there have been phenomenological studies with texture one-zero [8–10], two-zeros [11–24] and more within the context of Pontecorvo Maki Nakagawa Sakata (PMNS), tribimaximal (TB), and trimaximal (TM) mixing matrix. Similarly, in Refs. [25–30], the authors have studied the phenomenological implication of vanishing minors in the neutrino mass matrix. Moreover, in Refs. [31–36] and Refs. [37–41], the authors have explored the implication of cofactor zero and hybrid texture of the neutrino mass matrix. In case of zero textures, it is found that three or more zeros in the neutrino mass matrix cannot accommodate the current neutrino oscillation data. In Ref. [11], the authors have found that out of fifteen possible two texture zeros cases only seven cases with PMNS mixing are allowed experimentally. Also out of fifteen possible two cofactors zero patterns only seven patterns are acceptable [25]. In case of TM mixing along with magic symmetry [22], the authors have found that only two cases are valid for two texture zero. TM mixing with one texture zero was studied in Ref. [10] and found that all six patterns are compatible with current neutrino oscillation data. For TB mixing along with the condition of texture zeros or vanishing minor [28] only five patterns are allowed. In this work we study the implication of one vanishing minor in the neutrino mass matrix using trimaximal mixing.

Our paper is organized as follows. In Sec. II, we briefly discuss the neutrino mass matrix using trimaximal mixing matrix. We find all the mixing parameters such as θ_{13}, θ_{23}, θ_{12} and the CP violating parameter δ_{CP} in terms of the unknown parameters θ and ϕ of the trimaximal mixing matrix. In Sec. III, we describe the formalism of one vanishing minor in the neutrino mass matrix and identify all the possible patterns of one vanishing minor. We provide all the detail numerical analysis and discussion of each pattern in Secs. IV and V. The fine-tuning of the neutrino mass matrix is presented in Sec. VI. In Sec. VII, we present the symmetry realization and conclude in Sec. VIII.

II. NEUTRINO MASS MATRIX

The most widely studied lepton flavor mixing is TB mixing pattern [42–45] introduced by Harrison, Perkins, and Scott. TB mixing pattern provides remarkable agreement with the atmospheric and solar neutrino oscillation data. The TB mixing pattern is given by

$$U_{TB} = \begin{pmatrix} \sqrt{\frac{2}{3}} & \sqrt{\frac{1}{3}} & 0 \\ -\sqrt{\frac{1}{6}} & \sqrt{\frac{1}{3}} & \sqrt{\frac{1}{2}} \\ -\sqrt{\frac{1}{6}} & \sqrt{\frac{1}{3}} & -\sqrt{\frac{1}{2}} \end{pmatrix}. \tag{1}$$

The TB mixing matrix possesses two types of symmetries: $\mu-\tau$ symmetry and magic symmetry. Although TB mixing matrix correctly predicted the value of atmospheric mixing angle θ_{23} and the solar mixing angle θ_{12}, it, however, failed to explain a nonzero value of the reactor mixing angle θ_{13} that was experimentally confirmed by T2K [46], MINOS [47], Double Chooz [48], Daya Bay [49] and RENO [50] experiments. The possibility of an exact $\mu-\tau$ symmetry in the mass matrix was completely ruled out by a relatively large value of θ_{13}. Modifications in the TB mixing pattern [51–53] was made to accommodate the present data. The TM mixing matrix was constructed by multiplying the TB mixing matrix by an unitary matrix and can be written as

$$U_{TM_1} = \begin{pmatrix} \sqrt{\frac{2}{3}} & \frac{1}{\sqrt{3}}\cos\theta & \frac{1}{\sqrt{3}}\sin\theta \\ -\frac{1}{\sqrt{6}} & \frac{\cos\theta}{\sqrt{3}} - \frac{e^{i\phi}\sin\theta}{\sqrt{2}} & \frac{\sin\theta}{\sqrt{3}} + \frac{e^{i\phi}\cos\theta}{\sqrt{2}} \\ -\frac{1}{\sqrt{6}} & \frac{\cos\theta}{\sqrt{3}} + \frac{e^{i\phi}\sin\theta}{\sqrt{2}} & \frac{\sin\theta}{\sqrt{3}} - \frac{e^{i\phi}\cos\theta}{\sqrt{2}} \end{pmatrix}. \tag{2}$$

and

$$U_{TM_2} = \begin{pmatrix} \sqrt{\frac{2}{3}}\cos\theta & \frac{1}{\sqrt{3}} & \sqrt{\frac{2}{3}}\sin\theta \\ -\frac{\cos\theta}{\sqrt{6}} + \frac{e^{-i\phi}\sin\theta}{\sqrt{2}} & \frac{1}{\sqrt{3}} & -\frac{\sin\theta}{\sqrt{6}} - \frac{e^{-i\phi}\cos\theta}{\sqrt{2}} \\ -\frac{\cos\theta}{\sqrt{6}} - \frac{e^{-i\phi}\sin\theta}{\sqrt{2}} & \frac{1}{\sqrt{3}} & -\frac{\sin\theta}{\sqrt{6}} + \frac{e^{-i\phi}\cos\theta}{\sqrt{2}} \end{pmatrix}. \tag{3}$$

where θ and ϕ are two free parameters. The neutrino mass matrix corresponding to TM mixing matrix can be written as

$$M_{\rho\sigma} = (V M_{\text{diag}} V^T)_{\rho\sigma} \quad \text{with} \quad \rho,\sigma = e,\mu,\tau, \tag{4}$$

where $M_{\text{diag}} = \text{diag}(m_1, m_2, m_3)$ is the diagonal matrix containing three mass state, $V = U_{TM}P$ and P is the phase matrix written as

$$P = \begin{pmatrix} 1 & 0 & 0 \\ 0 & e^{i\alpha} & 0 \\ 0 & 0 & e^{i\beta} \end{pmatrix}. \tag{5}$$

Here α and β are the two CP violating Majorana phases.

A. TM_1 mixing matrix

With TM_1 mixing matrix, the elements of the neutrino mass matrix can be written as

$$\begin{aligned}
M_{ee} &= \frac{2}{3}m_1 + \frac{1}{3}\cos^2\theta m_2 e^{2i\alpha} + \frac{1}{3}\sin^2\theta m_3 e^{2i\beta}, \\
M_{e\mu} &= \left(-\frac{1}{3}\right)m_1 + \left(\frac{1}{3}\cos^2\theta - \frac{1}{\sqrt{6}}\sin\theta\cos\theta e^{i\phi}\right)m_2 e^{2i\alpha} + \left(\frac{1}{3}\sin^2\theta + \frac{1}{\sqrt{6}}\sin\theta\cos\theta e^{i\phi}\right)m_3 e^{2i\beta}, \\
M_{e\tau} &= \left(-\frac{1}{3}\right)m_1 + \left(\frac{1}{3}\cos^2\theta + \frac{1}{\sqrt{6}}\sin\theta\cos\theta e^{i\phi}\right)m_2 e^{2i\alpha} + \left(\frac{1}{3}\sin^2\theta - \frac{1}{\sqrt{6}}\sin\theta\cos\theta e^{i\phi}\right)m_3 e^{2i\beta}, \\
M_{\mu\mu} &= \frac{1}{6}m_1 + \left(\frac{1}{\sqrt{3}}\cos\theta - \frac{1}{\sqrt{2}}\sin\theta e^{i\phi}\right)^2 m_2 e^{2i\alpha} + \left(\frac{1}{\sqrt{3}}\sin\theta + \frac{1}{\sqrt{2}}\cos\theta e^{i\phi}\right)^2 m_3 e^{2i\beta}, \\
M_{\mu\tau} &= \frac{1}{6}m_1 + \left(\frac{1}{3}\cos^2\theta - \frac{1}{2}\sin^2\theta e^{2i\phi}\right)m_2 e^{2i\alpha} + \left(\frac{1}{3}\sin^2\theta - \frac{1}{2}\cos^2\theta e^{2i\phi}\right)m_3 e^{2i\beta}, \\
M_{\tau\tau} &= \frac{1}{6}m_1 + \left(\frac{1}{\sqrt{3}}\cos\theta + \frac{1}{\sqrt{2}}\sin\theta e^{i\phi}\right)^2 e^{2i\alpha} + \left(\frac{1}{\sqrt{3}}\sin\theta - \frac{1}{\sqrt{2}}\cos\theta e^{i\phi}\right)^2 m_3 e^{2i\beta}.
\end{aligned} \tag{6}$$

The three neutrino mixing angles θ_{12}, θ_{23}, and θ_{13} can be expressed in terms of θ and ϕ, the free parameters of the TM_1 matrix, as

$$\begin{aligned}
s_{12}^2 &= \frac{|(U_{12})_{TM_1}|^2}{1-|(U_{13})_{TM_1}|^2} = 1 - \frac{2}{3-\sin^2\theta}, \\
s_{23}^2 &= \frac{|(U_{23})_{TM_1}|^2}{1-|(U_{13})_{TM_1}|^2} = \frac{1}{2}\left(1 + \frac{\sqrt{6}\sin 2\theta\cos\phi}{3-\sin^2\theta}\right), \\
s_{13}^2 &= |(U_{13})_{TM_1}|^2 = \frac{1}{3}\sin^2\theta,
\end{aligned} \tag{7}$$

where $s_{ij} = \sin\theta_{ij}$ and $c_{ij} = \cos\theta_{ij}$ for $i, j = 1, 2, 3$. Using the standard parametrization of the PMNS matrix, the Jarlskog invariant, a measure of CP violation, is defined as [54]

$$J = s_{12}s_{13}s_{23}c_{12}c_{13}^2c_{23}\sin\delta. \tag{8}$$

Again, using the elements from TM_1 mixing matrix, the Jarlskog invariant can be expressed as

$$J = \frac{1}{6\sqrt{6}}\sin 2\theta\sin\phi. \tag{9}$$

Combining Eqs. (8) and (9), we can write δ in terms of θ and ϕ as

$$\csc^2\delta = \csc^2\phi - \frac{6\sin^2 2\theta\cot^2\phi}{(3-\sin^2\theta)^2}. \tag{10}$$

The nature of neutrino can be determined from the effective Majorana mass term. It also measures the rate of neutrinoless double beta decay. The effective Majorana mass $|M_{ee}|$ for the TM_1 mixing matrix can be written as

$$|M_{ee}| = \left|\frac{1}{3}(2m_1 + m_2\cos^2\theta e^{2i\alpha} + m_3\sin^2\theta e^{2i\beta})\right|. \tag{11}$$

Similarly, the effective electron antineutrino mass can be expressed as

$$M_\nu^2 = \sum_{i=1}^{3} U_{ie}^2 = \frac{1}{3}(2m_1^2 + m_2^2\cos^2\theta + m_3^2\sin^2\theta). \tag{12}$$

B. TM_2 mixing matrix

Using TM_2 mixing matrix, we can write the elements of the neutrino mass matrix as

$$
\begin{aligned}
M_{ee} &= \left(\frac{2}{3}\cos^2\theta\right)m_1 + \frac{1}{3}m_2e^{2i\alpha} + \left(\frac{2}{3}\sin^2\theta\right)m_3e^{2i\beta},\\
M_{e\mu} &= \left(-\frac{1}{3}\cos^2\theta + \frac{1}{\sqrt{3}}\sin\theta\cos\theta e^{-i\phi}\right)m_1 + \frac{1}{3}m_2e^{2i\alpha} + \left(-\frac{1}{3}\sin^2\theta - \frac{1}{\sqrt{3}}\sin\theta\cos\theta e^{-i\phi}\right)m_3e^{2i\beta},\\
M_{e\tau} &= \left(-\frac{1}{3}\cos^2\theta - \frac{1}{\sqrt{3}}\sin\theta\cos\theta e^{-i\phi}\right)m_1 + \frac{1}{3}m_2e^{2i\alpha} + \left(-\frac{1}{3}\sin^2\theta + \frac{1}{\sqrt{3}}\sin\theta\cos\theta e^{-i\phi}\right)m_3e^{2i\beta},\\
M_{\mu\mu} &= \left(-\frac{1}{\sqrt{6}}\cos\theta + \frac{1}{\sqrt{2}}\sin\theta e^{-i\phi}\right)^2m_1 + \frac{1}{3}m_2e^{2i\alpha} + \left(\frac{1}{\sqrt{6}}\sin\theta + \frac{1}{\sqrt{2}}\cos\theta e^{-i\phi}\right)^2m_3e^{2i\beta},\\
M_{\mu\tau} &= \left(\frac{1}{6}\cos^2\theta - \frac{1}{2}\sin^2\theta e^{-2i\phi}\right)m_1 + \frac{1}{3}m_2e^{2i\alpha} + \left(\frac{1}{6}\sin^2\theta - \frac{1}{2}\cos^2\theta e^{-2i\phi}\right)m_3e^{2i\beta},\\
M_{\tau\tau} &= \left(\frac{1}{\sqrt{6}}\cos\theta + \frac{1}{\sqrt{2}}\sin\theta e^{-i\phi}\right)^2m_1 + \frac{1}{3}m_2e^{2i\alpha} + \left(-\frac{1}{\sqrt{6}}\sin\theta + \frac{1}{\sqrt{2}}\cos\theta e^{-i\phi}\right)^2m_3e^{2i\beta}.
\end{aligned}
\tag{13}
$$

The three neutrino mixing angles θ_{12}, θ_{23}, and θ_{13} can be expressed as

$$
\begin{aligned}
s_{12}^2 &= \frac{1}{3-2\sin^2\theta},\\
s_{23}^2 &= \frac{1}{2}\left(1 + \frac{\sqrt{3}\sin 2\theta\cos\phi}{3-2\sin^2\theta}\right),\\
s_{13}^2 &= \frac{2}{3}\sin^2\theta.
\end{aligned}
\tag{14}
$$

Again, using the elements from the TM_2 mixing matrix, the Jarlskog invariant can be expressed as

$$
J = \frac{1}{6\sqrt{3}}\sin 2\theta\sin\phi. \tag{15}
$$

We can express the Dirac CP violating parameter δ_{CP} in terms of θ and ϕ as

$$
\csc^2\delta = \csc^2\phi - \frac{3\sin^2 2\theta\cot^2\phi}{(3-2\sin^2\theta)^2}. \tag{16}
$$

The effective Majorana mass $|M_{ee}|$ for the TM_2 mixing matrix can be written as

$$
|M_{ee}| = \left|\frac{1}{3}(2m_1\cos^2\theta + m_2e^{2i\alpha} + 2m_3\sin^2\theta e^{2i\beta})\right|. \tag{17}
$$

The effective electron antineutrino mass can be expressed as

$$
M_\nu^2 = \frac{1}{3}(2m_1^2 + m_2^2\cos^2\theta + 2m_3^2\sin^2\theta). \tag{18}
$$

III. ONE VANISHING MINOR IN NEUTRINO MASS MATRIX

There are six independent minors corresponding to six independent elements in the neutrino mass matrix. We denote the minor corresponding to ijth element of M_{ij} as C_{ij}. The six possible patterns of one minor zero in the neutrino mass matrix are listed in Table I. The condition for one vanishing minor can be written as

$$
M_{ab}M_{cd} - M_{uv}M_{wx} = 0. \tag{19}
$$

More specifically, we can write Eq. (19) in terms of a complex equation as

$$
m_1m_2X_3e^{2i\alpha} + m_2m_3X_1e^{2i(\alpha+\beta)} + m_3m_1X_2e^{2i\beta} = 0, \tag{20}
$$

where

$$
X_k = (U_{ai}U_{bi}U_{cj}U_{dj} - U_{ui}U_{vi}U_{wj}U_{xj}) + (i \leftrightarrow j), \tag{21}
$$

with (i, j, k) as the cyclic permutation of (1,2,3). Using Eq. (20), one can write the two mass ratios as

$$
\begin{aligned}
\frac{m_1}{m_2} &= \frac{\Re(X_3e^{2i\alpha})\Im(X_1e^{2i(\alpha+\beta)}) - \Re(X_1e^{2i(\alpha+\beta)})\Im(X_3e^{2i\alpha})}{\Re(X_2e^{2i\beta})\Im(X_3e^{2i\alpha}) - \Re(X_3e^{2i\alpha})\Im(X_2e^{2i\beta})},\\
\frac{m_3}{m_2} &= \frac{\Re(X_3e^{2i\alpha})\Im(X_1e^{2i(\alpha+\beta)}) - \Re(X_1e^{2i(\alpha+\beta)})\Im(X_3e^{2i\alpha})}{\Re(X_1e^{2i(\alpha+\beta)})\Im(X_2e^{2i\beta}) - \Re(X_2e^{2i\beta})\Im(X_1e^{2i(\alpha+\beta)})}.
\end{aligned}
\tag{22}
$$

TABLE I. One minor zero patterns.

Pattern	Constraining equation
I	$C_{33} = 0$
II	$C_{22} = 0$
III	$C_{31} = 0$
IV	$C_{21} = 0$
V	$C_{32} = 0$
VI	$C_{11} = 0$

The value of m_1, m_2, and m_3 can be calculated using Eq. (22) and mass square difference Δm^2_{21}. That is

$$m_1 = \sqrt{\Delta m^2_{21}}\sqrt{\frac{\left(\frac{m_1}{m_2}\right)^2}{\left|1-\left(\frac{m_1}{m_2}\right)^2\right|}},$$
$$m_2 = \sqrt{\Delta m^2_{21}}\sqrt{\frac{1}{\left|1-\left(\frac{m_1}{m_2}\right)^2\right|}},$$
$$m_3 = \sqrt{\Delta m^2_{21}}\sqrt{\frac{\left(\frac{m_3}{m_2}\right)^2}{\left|1-\left(\frac{m_1}{m_2}\right)^2\right|}}. \quad (23)$$

Similarly, the ratio of squared mass difference is defined as

$$r \equiv \left|\frac{\Delta m^2_{21}}{\Delta m^2_{32}}\right| = \left|\frac{1-\left(\frac{m_1}{m_2}\right)^2}{\left(\frac{m_3}{m_2}\right)^2-1}\right|, \quad (24)$$

where Δm^2_{21} and Δm^2_{32} represent solar and atmospheric mass squared difference, respectively. Value of $r = (2.950 \pm 0.08) \times 10^{-2}$ is determined by using the measured values of Δm^2_{21} and Δm^2_{32} reported in Ref. [55].

IV. RESULTS AND DISCUSSION

For our numerical analysis, we use the measured values of the oscillation parameters reported in Ref. [55]. For completeness, we report them in Table II. We wish to find the value of the unknown parameters θ and ϕ. It is evident from Eqs. (7) and (14) that the neutrino oscillation parameters θ_{12} and θ_{13} depend only on θ. To find the best fit value of θ, we perform a naive χ^2 analysis. The relevant χ^2 is defined as

$$\chi^2(\theta) = \sum_{i=1}^{2} \frac{(\theta_i^{\rm cal} - \theta_i^{\rm exp})^2}{(\sigma_i^{\rm exp})^2}, \quad (25)$$

where $\theta_i = (\theta_{12}, \theta_{13})$. Here $\theta_i^{\rm cal}$ represents the theoretical value of θ_i and $\theta_i^{\rm exp}$ represents measured central value of θ_i. The corresponding uncertainties in the measured value of θ_i is represented by $\sigma_i^{\rm exp}$.

For the TM_1 mixing matrix, the best fit value of θ is obtained to be 14.96°. The corresponding best fit values of θ_{12} and θ_{13} are 34.33° and 8.57°, respectively. The 3σ allowed range of θ is found to be (14.26°–15.64°). Using the allowed range of θ, we obtain the allowed ranges of θ_{12} and θ_{23} to be (34.25°–34.42°) and (32.11°–57.88°), respectively. We show in Fig. 1(a) the correlation of θ_{13} and θ_{12} for the TM_1 mixing matrix. To see the variation of θ_{23} with ϕ, we use the allowed range of θ and vary ϕ within its full range from 0° to 360°. We show in Fig. 1(b) the variation of θ_{23} as a function of the unknown parameter ϕ. We also obtain the best fit value of ϕ by using the measured best fit value of θ_{23}. The best fit value is shown with a * mark in Fig. 1(b). The best fit values of ϕ corresponding to the best fit value of $\theta_{23} = 49.2°$ are 69.43° and 290.57°, respectively. We show the variation of J and δ as a function of ϕ in Figs. 1(c) and 1(d), respectively. It is observed that the Jarlskog rephasing invariant J and the Dirac CP violating phase δ are restricted to two regions. The corresponding best fit values of J and δ are $[-3.184 \times 10^{-2}, 3.185 \times 10^{-2}]$ and [71.11°, 288.98°], respectively. We also obtain the 3σ allowed ranges of J and δ to be $[0, \pm 3.53 \times 10^{-2}]$ and [(55.05, 124.95)°, (235.05, 304.95)°], respectively.

For TM_2 mixing matrix, the best fit value of θ is obtained to be 10.50°. The corresponding best fit values of θ_{12} and θ_{13} are 35.72° and 8.56°, respectively. The 3σ allowed range of θ is found to be (10.03°–10.99°). Using the allowed range of θ, we obtain the allowed ranges of θ_{12} and θ_{23} to be (35.68°–35.76°) and (39.50°–51.40°), respectively. It should be noted that although the allowed range of θ_{12} obtained with TM_2 mixing matrix is consistent with the 3σ experimental range, the best fit value obtained for θ_{12}, however, deviates from the experimental best fit value at more than 2σ significance. This is quite a generic feature of TM_2 mixing matrix because, by default, value of θ_{12} will be greater than or equal to the value obtained in case of TB mixing matrix. We show in Fig. 2(a) the correlation of θ_{13} and θ_{12} for the TM_2 mixing matrix.

TABLE II. Neutrino oscillation parameters from NuFIT [55].

	Normal ordering (best fit)		Inverted ordering ($\Delta\chi^2 = 7.1$)	
Parameter	bfp $\pm 1\sigma$	3σ ranges	bfp $\pm 1\sigma$	3σ ranges
θ_{12}°	$33.44^{+0.77}_{-0.74}$	$31.27 \to 35.86$	$33.45^{+0.77}_{-0.74}$	$31.27 \to 35.87$
θ_{23}°	$49.2^{+1.0}_{-1.3}$	$39.5 \to 52.0$	$49.5^{+1.0}_{-1.2}$	$39.8 \to 52.1$
θ_{13}°	$8.57^{+0.13}_{-0.12}$	$8.20 \to 8.97$	$8.60^{+0.12}_{-0.12}$	$8.24 \to 8.98$
δ°	194^{+52}_{-25}	$105 \to 405$	287^{+27}_{-32}	$192 \to 361$
$\frac{\Delta m^2_{21}}{10^{-5}\ \mathrm{eV}^2}$	$7.42^{+0.21}_{-0.20}$	$6.82 \to 8.04$	$7.42^{+0.21}_{-0.20}$	$6.82 \to 8.04$
$\frac{\Delta m^2_{3l}}{10^{-3}\ \mathrm{eV}^2}$	$+2.515^{+0.028}_{-0.028}$	$+2.431 \to +2.599$	$-2.498^{+0.028}_{-0.029}$	$-2.584 \to -2.413$

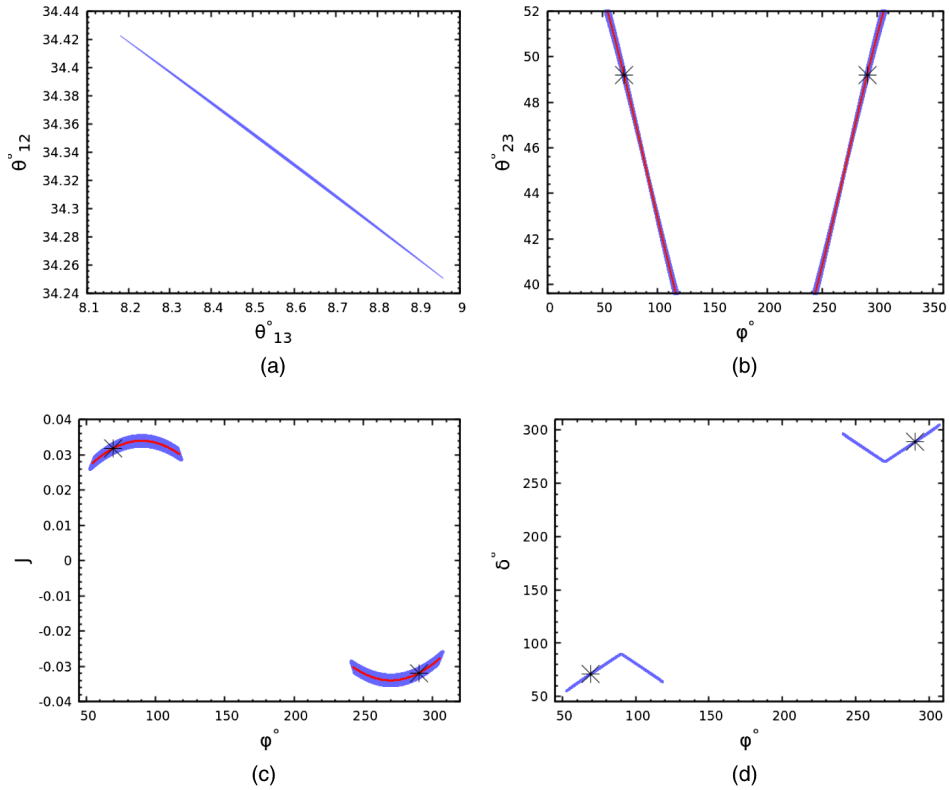

FIG. 1. (a) Correlation of θ_{13} and θ_{12}, (b) variation of θ_{23} as a function of ϕ, (c) variation of J as a function of ϕ, and (d) variation of δ as a function of ϕ for TM_1 mixing matrix.

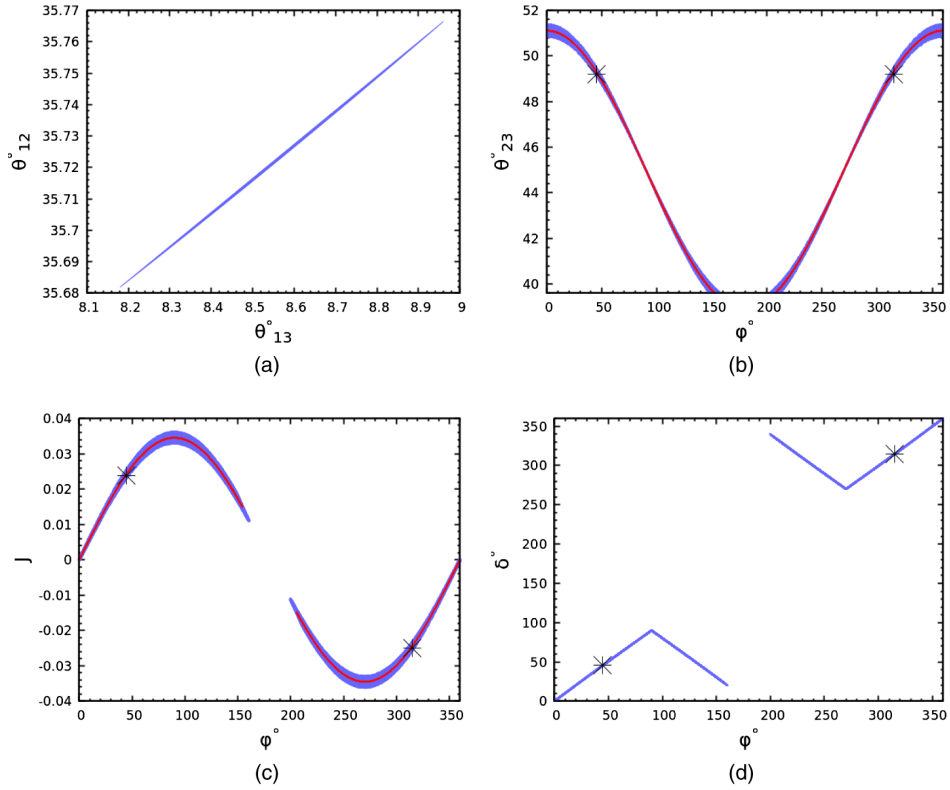

FIG. 2. (a) Correlation of θ_{13} and θ_{12}, (b) variation of θ_{23} as a function of ϕ, (c) variation of J as a function of ϕ, and (d) variation of δ as a function of ϕ for TM_2 mixing matrix.

To see the variation of θ_{23} with ϕ, we use the allowed range of θ and vary ϕ within its full range from 0° to 360°. We show in Fig. 2(b) the variation of θ_{23} as a function of the unknown parameter ϕ. The best fit value is shown with a * mark in Fig. 2(b). We obtain the best fit value of ϕ by using the measured best fit value of θ_{23}. The best fit values of ϕ corresponding to the best fit value of $\theta_{23} = 49.2°$ are 44.86° and 315.19°, respectively. We get two best fit values of ϕ because θ_{23} is invariant under the transformation $\phi \to (2\pi - \phi)$ which is evident from Eqs. (7) and (14). We also show the variation of J and δ as a function of ϕ in Figs. 2(c) and 2(d), respectively. It is observed that the Jarlskog rephasing invariant J and the Dirac CP violating phase δ are restricted to two regions. The corresponding best fit values of J and δ are $[2.37 \times 10^{-2}, -2.50 \times 10^{-2}]$ and [45.48°, 314.44°], respectively. We also obtain the 3σ allowed ranges of J and δ to be $[0, \pm 3.60 \times 10^{-2}]$ and [(0,90)°, (270,360)°], respectively.

In case of inverted mass ordering the 3σ allowed range of θ are found to be (14.37°–15.64°) and (10.10°–10.99°) for both TM_1 and TM_2 mixing matrix, respectively. Using the 3σ allowed range of θ, we obtain the 3σ allowed ranges of θ_{12} to be (34.25°–34.41°) and (35.68°–35.76°), respectively for both TM_1 and TM_2 mixing matrix. The 3σ allowed ranges of θ_{23} to be (32.12°–57.87°) and (38.60°–51.39°), respectively for both TM_1 and TM_2 mixing matrix. It is to be noted that the mixing angles are almost similar for both the normal and inverted mass ordering. So for our later discussion we will use the values of mixing angles for the normal mass ordering reported in Ref. [55].

V. PHENOMENOLOGY OF ONE VANISHING MINOR

We wish to investigate the phenomenological implication of one vanishing minor in the neutrino mass matrix on the total neutrino mass, the effective Majorana mass term and the electron antineutrino mass. It is evident from Eq. (23) that neutrino mass m_i depends on θ, ϕ, α, β, and the mass squared difference Δm^2_{21}. We use the best fit value and the 3σ allowed range of θ and ϕ of Sec. IV that are determined by the measured values of the mixing angles θ_{13}, θ_{12}, and θ_{23}. The two unknown Majorana phases α and β are varied within their full range from 0° to 360°. Moreover, we use the 3σ allowed ranges of Δm^2_{21} and r to constrain the values of the neutrino masses. Now we proceed to analyze all the six patterns of one vanishing minor one by one.

A. Pattern I: $C_{33} = 0$

Let us first consider minor zero for the (3,3) element of the neutrino mass matrix. The equation corresponding to this pattern can be expressed in terms of the elements of the neutrino mass matrix as

$$(M_\nu)_{ee}(M_\nu)_{\mu\mu} - (M_\nu)_{e\mu}(M_\nu)_{e\mu} = 0. \tag{26}$$

Using Eq. (22), the two mass ratios for TM_1 can be expressed as

$$\frac{m_1}{m_2} = \frac{\mathcal{A}_1 \sin 2\beta + \mathcal{A}_2 \cos 2\beta}{(\mathcal{A}_3 + \mathcal{A}_4)\sin 2(\alpha - \beta) + (\mathcal{A}_5 - \mathcal{A}_6)\cos 2(\alpha - \beta)},$$
$$\frac{m_3}{m_2} = \frac{\mathcal{A}_1 \sin 2\beta + \mathcal{A}_2 \cos 2\beta}{\mathcal{A}_7 \sin 2\alpha + \mathcal{A}_8 \cos 2\alpha}, \tag{27}$$

Similarly, for TM_2 mixing matrix, the mass ratios can be expressed as

$$\frac{m_1}{m_2} = \frac{(\tilde{\mathcal{A}}_1 + \tilde{\mathcal{A}}_2)\sin 2(\beta - \phi) + (\tilde{\mathcal{A}}_3 + \tilde{\mathcal{A}}_4)\cos 2(\beta - \phi)}{\tilde{\mathcal{A}}_5 \sin 2(\alpha - \beta) - \tilde{\mathcal{A}}_6 \cos 2(\alpha - \beta)},$$
$$\frac{m_3}{m_2} = \frac{(\tilde{\mathcal{A}}_1 + \tilde{\mathcal{A}}_2)\sin 2(\beta - \phi) + (\tilde{\mathcal{A}}_3 + \tilde{\mathcal{A}}_4)\cos 2(\beta - \phi)}{\tilde{\mathcal{A}}_7 \sin 2(\phi - \alpha) - \tilde{\mathcal{A}}_8 \cos 2(\phi - \alpha)}. \tag{28}$$

All the relevant expressions for $\mathcal{A}_i$ and $\tilde{\mathcal{A}}_i$ are reported in Eqs. (A1) and (A6) of appendix, respectively. We show the variation of neutrino masses m_1, m_2, and m_3 as a function of ϕ in Figs. 3(a) and 4(a) for TM_1 and TM_2 mixing matrix,

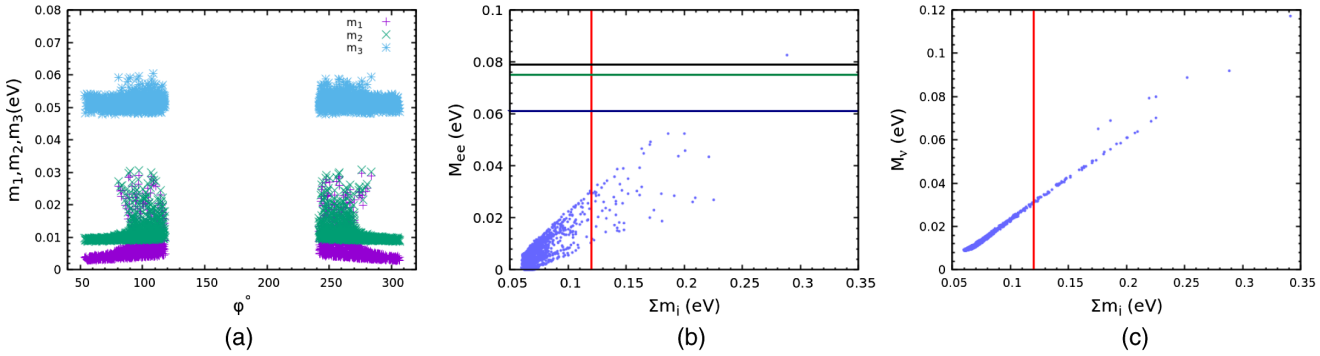

FIG. 3. (a) Variation of m_1, m_2, and m_3 as a function of ϕ, (b) correlation of $\sum m_i$ and m_{ee}, and (c) correlation of $\sum m_i$ and m_ν for C_{33} pattern using TM_1 mixing matrix. The vertical red line is the upper bound of the total neutrino mass reported in Ref. [3]. The black, green, and blue lines are the experimental upper bounds of the effective Majorana mass reported in Refs. [4–7].

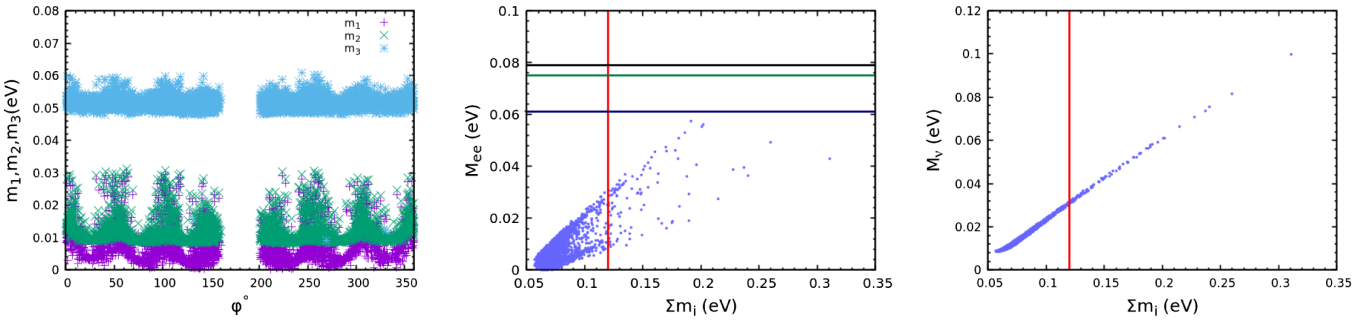

FIG. 4. (a) Variation of m_1, m_2, and m_3 as a function of ϕ, (b) correlation of $\sum m_i$ and m_{ee} , and (c) correlation of $\sum m_i$ and m_ν for C_{33} pattern using TM_2 mixing matrix. The vertical red line represents the upper bound of $\sum m_i$ reported in Ref. [3]. The black, green, and blue lines are the experimental upper bounds of M_{ee} obtained from Refs. [4–7].

respectively. It shows normal mass ordering for TM_1 mixing matrix while for TM_2 mixing matrix, it shows both normal and inverted mass ordering. The correlation of M_{ee} and $\sum m_i$ for TM_1 and TM_2 mixing matrix are shown in Figs. 3(b) and 4(b), respectively. The vertical red line shows the upper bound of the total neutrino mass reported in Ref. [3]. The black, green and blue lines are the experimental upper bounds of the effective Majorana mass as reported in Refs. [4–7]. In Figs. 3(c) and 4(c), we have shown the correlation of M_ν with $\sum m_i$ for TM_1 and TM_2 mixing matrix, respectively. It is observed that the total neutrino mass $\sum m_i$ puts severe constraints on effective Majorana mass and M_ν.

The range of the absolute neutrino mass scale, the effective Majorana neutrino mass and the effective electron antineutrino mass obtained for both the mixing matrix are listed in Table III. The calculated upper bound of m_{ee} is obtained to be of $\mathcal{O}(10^{-2})$ which is within the reach of neutrinoless double beta decay experiment. The calculated upper bound of $m_\nu < 0.06$ eV may not be within the reach of KATRIN experiment. It may, however, be within the reach of next generation experiment such as Project 8. It should, however, be mentioned that once the total neutrino mass constraint is imposed, the calculated upper bound of m_{ee} and m_ν is found to be less than 0.04 eV.

B. Pattern II: $C_{22} = 0$

The vanishing minor condition for this pattern corresponding to element (2,2) is given by

$$(M_\nu)_{ee}(M_\nu)_{\tau\tau} - (M_\nu)_{e\tau}(M_\nu)_{e\tau} = 0. \tag{29}$$

The two mass ratios for TM_1 and TM_2 mixing matrix can be expressed as

$$\frac{m_1}{m_2} = \frac{\mathcal{B}_1 \sin 2\beta + \mathcal{B}_2 \cos 2\beta}{(\mathcal{B}_3 + \mathcal{B}_4)\sin 2(\alpha-\beta) - (\mathcal{B}_5 - \mathcal{B}_6)\cos 2(\alpha-\beta)},$$
$$\frac{m_3}{m_2} = \frac{\mathcal{B}_1 \sin 2\beta + \mathcal{B}_2 \cos 2\beta}{\mathcal{B}_7 \sin 2\alpha + \mathcal{B}_8 \cos 2\alpha}, \tag{30}$$

and

$$\frac{m_1}{m_2} = \frac{(\tilde{\mathcal{B}}_1 + \tilde{\mathcal{B}}_2)\sin 2(\beta-\phi) + (\tilde{\mathcal{B}}_3 + \tilde{\mathcal{B}}_4)\cos 2(\beta-\phi)}{\tilde{\mathcal{B}}_5 \sin 2(\alpha-\beta) - \tilde{\mathcal{B}}_6 \cos 2(\alpha-\beta)},$$
$$\frac{m_3}{m_2} = \frac{(\tilde{\mathcal{B}}_1 + \tilde{\mathcal{B}}_2)\sin 2(\beta-\phi) + (\tilde{\mathcal{B}}_3 + \tilde{\mathcal{B}}_4)\cos 2(\beta-\phi)}{\tilde{\mathcal{B}}_7 \sin 2(\phi-\alpha) - \tilde{\mathcal{B}}_8 \cos 2(\phi-\alpha)}. \tag{31}$$

All the relevant expressions for $\mathcal{B}_i$ and $\tilde{\mathcal{B}}_i$ are reported in Eqs. (A2) and (A7) of appendix. We show the variation of neutrino masses m_1, m_2, and m_3 as a function of ϕ in Figs. 5(a) and 6(a) for TM_1 and TM_2 mixing matrix, respectively. It shows normal mass ordering for TM_1 mixing matrix while for TM_2 mixing matrix, it shows both normal and inverted mass ordering. The correlation of M_{ee} and $\sum m_i$ for TM_1 and TM_2 mixing matrix are shown in Figs. 5(b) and 6(b), respectively. In Figs. 5(c) and 6(c), we have shown the correlation of M_ν with $\sum m_i$ for TM_1 and TM_2 mixing matrix, respectively. The phenomenology of this pattern is quite similar to C_{33}.

The allowed range of the absolute neutrino mass scale, the effective Majorana mass and the effective electron

TABLE III. Allowed range of $\sum m_i$, m_{ee}, and m_ν for C_{33} pattern.

Mixing matrix	Mass ordering	$\sum m_i$ (eV)	m_{ee} (eV)	m_ν (eV)
TM_1	**NO**	[0.059, 0.288]	$[1.955 \times 10^{-5}, 0.048]$	$[8.889 \times 10^{-3}, 0.053]$
TM_2	**NO**	[0.056, 0.310]	$[1.462 \times 10^{-5}, 0.057]$	$[8.575 \times 10^{-3}, 0.099]$
	IO	[0.094, 0.425]	[0.014, 0.116]	[0.044, 0.144]

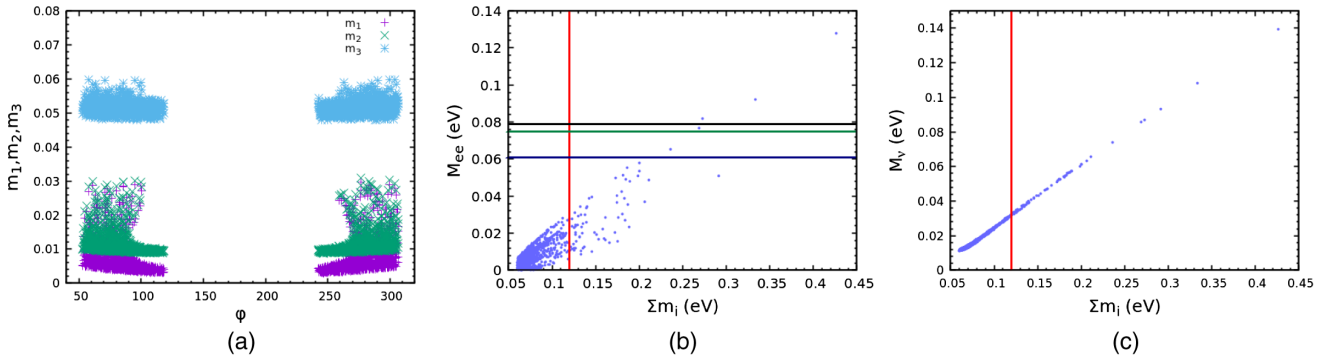

FIG. 5. (a) Variation of m_1, m_2, and m_3 as a function of ϕ, (b) correlation of $\sum m_i$ and m_{ee}, and (c) correlation of $\sum m_i$ and m_ν for C_{22} pattern using TM_1 mixing matrix. The vertical red line shows the upper bound of the total neutrino mass reported in Ref. [3]. The black, green, and blue lines are the experimental upper bounds of the effective Majorana mass reported in Refs. [4–7].

antineutrino mass for this pattern are listed in Table IV. It is evident from Figs. 5 and 6 that the upper bound of $\sum m_i < 1.2$ eV put severe constraint on the value of the effective Majorana mass term m_{ee} and the value of the effective electron antineutrino mass m_ν. The estimated upper bound of m_{ee} and m_ν is found to be less than 0.04 eV.

C. Pattern III: $C_{31} = 0$

This pattern corresponds to the matrix element (3,1) of the neutrino mass matrix. The vanishing minor condition is given by

$$(M_\nu)_{e\mu}(M_\nu)_{\mu\tau} - (M_\nu)_{e\tau}(M_\nu)_{\mu\mu} = 0. \tag{32}$$

Using the elements from the neutrino mass matrix, one can write the neutrino mass ratios for this pattern. With TM_1 mixing matrix, we have

$$\frac{m_1}{m_2} = \frac{\mathcal{C}_1 \sin 2\beta + \mathcal{C}_2 \cos 2\beta}{\mathcal{C}_3 \sin 2(\alpha-\beta) - \mathcal{C}_4 \cos 2(\alpha-\beta)},$$
$$\frac{m_3}{m_2} = \frac{\mathcal{C}_1 \sin 2\beta + \mathcal{C}_2 \cos 2\beta}{\mathcal{C}_5 \sin 2\alpha + \mathcal{C}_6 \cos 2\alpha}, \tag{33}$$

and for TM_2 mixing matrix, we have

$$\frac{m_1}{m_2} = \frac{\tilde{\mathcal{C}}_1 \sin 2(\beta-\phi) + \tilde{\mathcal{C}}_2 \cos 2(\beta-\phi)}{\tilde{\mathcal{C}}_3 \sin 2(\alpha-\beta) - \tilde{\mathcal{C}}_4 \cos 2(\alpha-\beta)},$$
$$\frac{m_3}{m_2} = \frac{\tilde{\mathcal{C}}_1 \sin 2(\beta-\phi) + \tilde{\mathcal{C}}_2 \cos 2(\beta-\phi)}{\tilde{\mathcal{C}}_5 \sin 2(\phi-\alpha) + \tilde{\mathcal{C}}_6 \cos 2(\phi-\alpha)}, \tag{34}$$

where all the relevant $\mathcal{C}_i$ and $\tilde{\mathcal{C}}_i$ are reported in Eqs. (A3) and (A8) of appendix. We show in Figs. 7(a) and 8(a) the correlation of neutrino masses m_1, m_2 and m_3 with the unknown parameter ϕ for TM_1 and TM_2 mixing matrix. It shows both normal and inverted mass ordering for TM_1 and TM_2 mixing matrix. Similarly, the correlation of M_{ee} against $\sum m_i$ for TM_1 and TM_2 mixing patterns are shown in Figs. 7(b) and 8(b), respectively. Moreover, in the Figs. 7(c) and 8(c), we have shown the correlation of M_ν with $\sum m_i$ for TM_1 and TM_2, respectively.

The allowed ranges of the absolute neutrino mass, the effective Majorana mass and the effective electron antineutrino mass for both the maxing matrix are listed in the Table V.

D. Pattern IV: $C_{21} = 0$

The vanishing minor condition for this pattern corresponding to element (2,1) of the neutrino mass matrix is given by

$$(M_\nu)_{\mu e}(M_\nu)_{\tau\tau} - (M_\nu)_{\tau e}(M_\nu)_{\mu\tau} = 0. \tag{35}$$

The two neutrino mass ratios for this pattern for TM_1 and TM_2 mixing matrix are given by

$$\frac{m_1}{m_2} = \frac{\mathcal{D}_1 \sin 2\beta + \mathcal{D}_2 \cos 2\beta}{\mathcal{D}_3 \sin 2(\alpha-\beta) + \mathcal{D}_4 \cos 2(\alpha-\beta)},$$
$$\frac{m_3}{m_2} = \frac{\mathcal{D}_1 \sin 2\beta + \mathcal{D}_2 \cos 2\beta}{\mathcal{D}_5 \sin 2\alpha + \mathcal{D}_6 \cos 2\alpha}, \tag{36}$$

and

TABLE IV. Allowed range of $\sum m_i$, m_{ee}, and m_ν for C_{22} pattern.

Mixing matrix	Mass ordering	$\sum m_i$ (eV)	m_{ee} (eV)	m_ν (eV)
TM_1	**NO**	[0.059, 0.425]	$[2.097 \times 10^{-5}, 0.127]$	[0.011, 0.139]
TM_2	**NO**	[0.056, 0.350]	$[4.185 \times 10^{-6}, 0.081]$	$[8.415 \times 10^{-3}, 0.113]$
	IO	[0.098, 0.427]	[0.015, 0.082]	[0.045, 0.145]

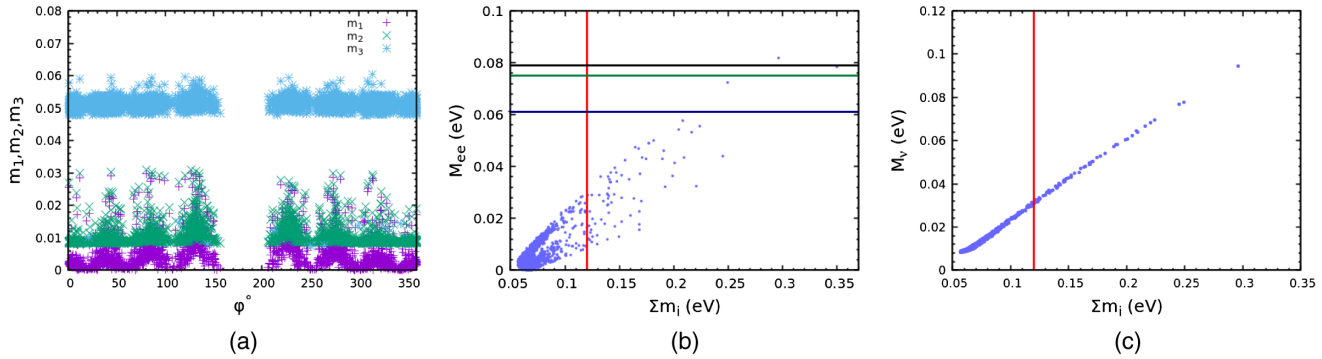

FIG. 6. (a) Variation of m_1, m_2, and m_3 as a function of ϕ, (b) correlation of $\sum m_i$ and m_{ee}, and (c) correlation of $\sum m_i$ and m_ν for C_{22} pattern using TM_2 mixing matrix. The vertical red line shows the upper bound of the total neutrino mass reported in Ref. [3]. The black, green, and blue lines show the experimental upper bounds of the effective Majorana mass reported in Refs. [4–7].

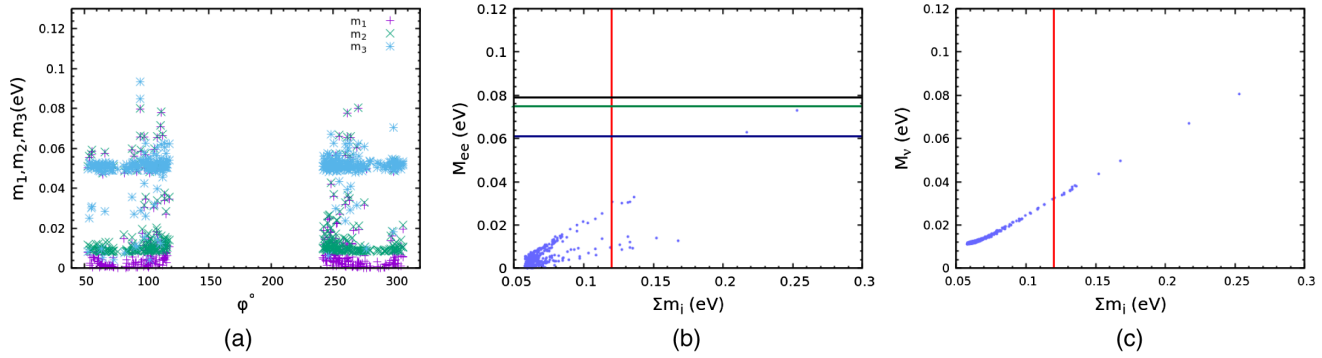

FIG. 7. (a) Variation of m_1, m_2, and m_3 as a function of ϕ, (b) correlation of $\sum m_i$ and m_{ee}, and (c) correlation of $\sum m_i$ and m_ν for C_{31} pattern using TM_1 mixing matrix. The vertical red line is the upper bound of the total neutrino mass reported in Ref. [3]. The black, green, and blue lines are the experimental upper bounds of the effective Majorana mass reported in Refs. [4–7].

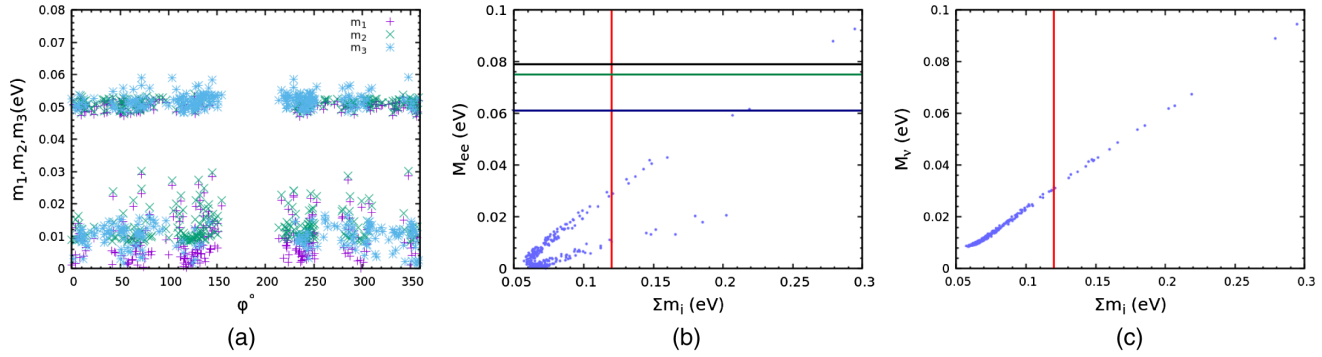

FIG. 8. (a) Variation of m_1, m_2, and m_3 as a function of ϕ, (b) correlation of $\sum m_i$ and m_{ee}, and (c) correlation of $\sum m_i$ and m_ν for C_{31} pattern using TM_2 mixing matrix. The vertical red line represents the upper bound of the total neutrino mass reported in Ref. [3]. The black, green, and blue lines represent the experimental upper bounds of the effective Majorana mass reported in Refs. [4–7].

TABLE V. Allowed range of $\sum m_i$, m_{ee}, and m_ν for C_{31} pattern.

Mixing matrix	Mass ordering	$\sum m_i$ (eV)	m_{ee} (eV)	m_ν (eV)
TM_1	**NO**	[0.057, 0.253]	$[1.003 \times 10^{-4}, 0.073]$	[0.011, 0.080
	IO	[0.096, 0.329]	[0.014, 0.087]	[0.044, 0.112]
TM_2	**NO**	[0.057, 0.294]	$[3.658 \times 10^{-5}, 0.092]$	$[8.624 \times 10^{-3}, 0.094]$
	IO	[0.092, 0.548]	[0.014, 0.126]	[0.045, 0.185]

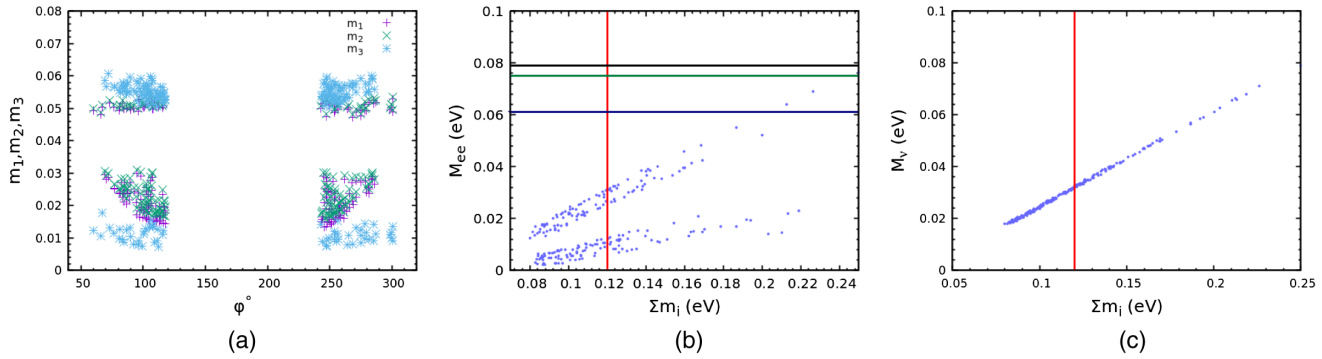

FIG. 9. (a) Variation of m_1, m_2, and m_3 as a function of ϕ, (b) correlation of $\sum m_i$ and m_{ee}, and (c) correlation of $\sum m_i$ and m_ν for C_{21} pattern using TM_1 mixing matrix. The vertical red line is the upper bound of the total neutrino mass reported in Ref. [3]. The black, green, and blue lines are the experimental upper bounds of the effective Majorana mass reported in Refs. [4–7].

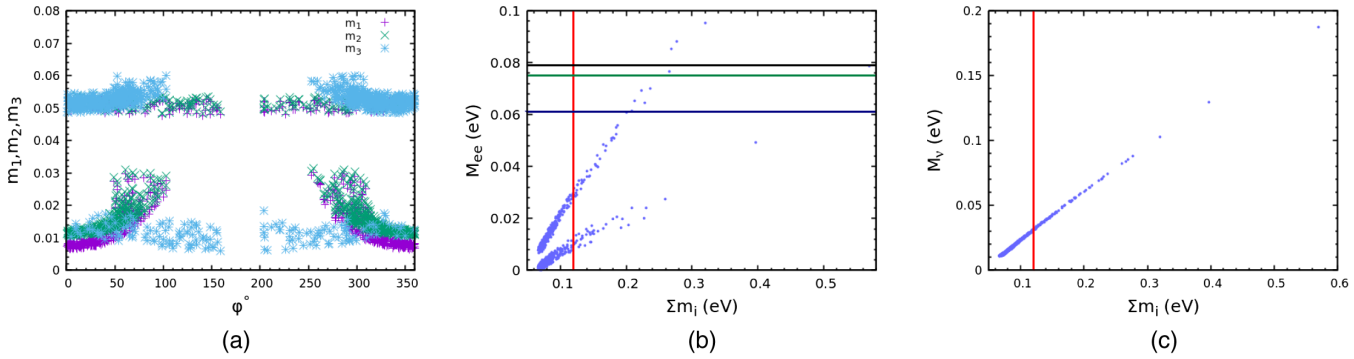

FIG. 10. (a) Variation of m_1, m_2, and m_3 as a function of ϕ, (b) correlation of $\sum m_i$ and m_{ee}, and (c) correlation of $\sum m_i$ and m_ν for C_{21} pattern using TM_2 mixing matrix. The vertical red line shows the upper bound of the total neutrino mass reported in Ref. [3]. The black, green, and blue lines show the experimental upper bounds of the effective Majorana mass reported in Refs. [4–7].

$$\frac{m_1}{m_2} = \frac{\tilde{\mathcal{D}}_1 \sin 2(\beta-\phi) + \tilde{\mathcal{D}}_2 \cos 2(\beta-\phi)}{\tilde{\mathcal{D}}_3 \sin 2(\alpha-\beta) + \tilde{\mathcal{D}}_4 \cos 2(\alpha-\beta)},$$
$$\frac{m_3}{m_2} = \frac{\tilde{\mathcal{D}}_1 \sin 2(\beta-\phi) + \tilde{\mathcal{D}}_2 \cos 2(\beta-\phi)}{\tilde{\mathcal{D}}_5 \sin 2(\phi-\alpha) - \tilde{\mathcal{D}}_6 \cos 2(\phi-\alpha)}, \quad (37)$$

where all the relevant $\mathcal{D}_i$ and $\tilde{\mathcal{D}}_i$ are reported in Eqs. (A4) and (A9) of appendix. In Figs. 9(a) and 10(a) we have shown the correlation of neutrino masses m_1, m_2, and m_3 with the unknown parameter ϕ for TM_1 and TM_2 mixing matrix. It shows both normal and inverted mass ordering for TM_1 and TM_2 mixing matrix. The correlation of M_{ee} against $\sum m_i$ for TM_1 and TM_2 mixing patterns are shown in Figs. 9(b) and 10(b), respectively. In the Figs. 9(c) and 10(c), we have shown the correlation of M_ν with $\sum m_i$ for TM_1 and TM_2, respectively.

We also report the allowed ranges of the absolute neutrino mass, the effective Majorana mass and the effective electron antineutrino mass for both the maxing matrix in Table VI. The phenomenology of this pattern is very similar to that of C_{31}.

E. Pattern V: $C_{32} = 0$

The condition of vanishing minor for this pattern is given by

$$(M_\nu)_{ee}(M_\nu)_{\mu\tau} - (M_\nu)_{\mu e}(M_\nu)_{e\tau} = 0. \quad (38)$$

TABLE VI. Allowed range of $\sum m_i$, m_{ee}, and m_ν for C_{21} pattern.

Mixing matrix	Mass ordering	$\sum m_i$ (eV)	m_{ee} (eV)	m_ν (eV)
TM_1	**NO**	[0.080, 0.249]	$[2.213 \times 10^{-3}, 0.076]$	[0.017, 0.079]
	IO	[0.101, 0.720]	[0.014, 0.125]	[0.044, 0.241]
TM_2	**NO**	[0.066, 0.569]	$[1.655 \times 10^{-4}, 0.095]$	[0.010, 0.187]
	IO	[0.097, 0.458]	[0.015, 0.137]	[0.045, 0.154]

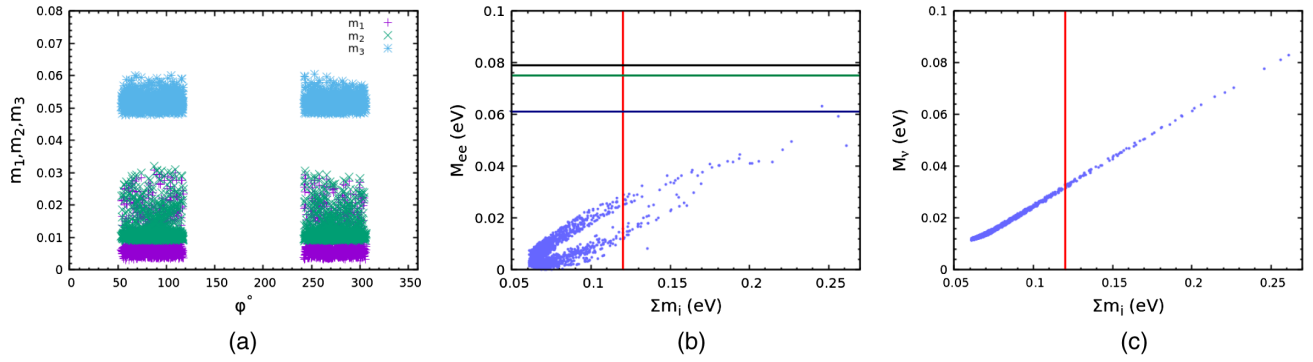

FIG. 11. (a) Variation of m_1, m_2, and m_3 as a function of ϕ, (b) correlation of $\sum m_i$ and m_{ee}, and (c) correlation of $\sum m_i$ and m_ν for C_{32} pattern using TM_1 mixing matrix. The vertical red line represents the upper bound of the total neutrino mass reported in Ref. [3]. The black, green, and blue lines represent the experimental upper bounds of the effective Majorana mass reported in Refs. [4–7].

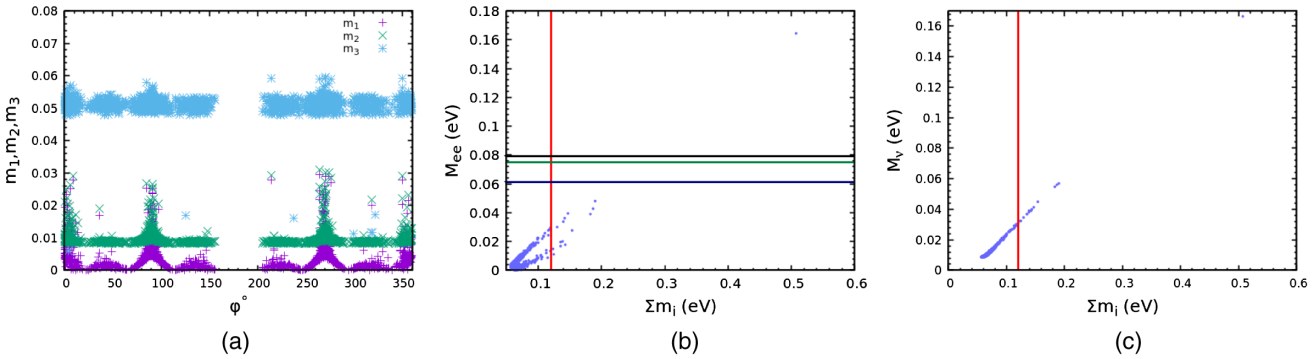

FIG. 12. (a) Variation of m_1, m_2, and m_3 as a function of ϕ, (b) correlation of $\sum m_i$ and m_{ee}, and (c) correlation of $\sum m_i$ and m_ν for C_{32} pattern using TM_2 mixing matrix. The vertical red line is the upper bound of the total neutrino mass reported in Ref. [3]. The black, green, and blue lines are the experimental upper bounds of the effective Majorana mass reported in Refs. [4–7].

For this pattern, the two neutrino mass ratios for TM_1 and TM_2 mixing matrix are given by

$$\frac{m_1}{m_2} = \frac{\mathcal{E}_1 \sin 2\beta + \mathcal{E}_2 \cos 2\beta}{\mathcal{E}_3 \sin 2(\alpha-\beta) + \mathcal{E}_4 \cos 2(\alpha-\beta)},$$
$$\frac{m_3}{m_2} = \frac{\mathcal{E}_1 \sin 2\beta + \mathcal{E}_2 \cos 2\beta}{\mathcal{E}_5 \sin 2\alpha + \mathcal{E}_6 \cos 2\alpha}, \tag{39}$$

and

$$\frac{m_1}{m_2} = \frac{\tilde{\mathcal{E}}_1 \sin 2(\beta-\phi) + \tilde{\mathcal{E}}_2 \cos 2(\beta-\phi)}{\tilde{\mathcal{E}}_3 \sin 2(\alpha-\beta) + \tilde{\mathcal{E}}_4 \cos 2(\alpha-\beta)},$$
$$\frac{m_3}{m_2} = \frac{\tilde{\mathcal{E}}_1 \sin 2(\beta-\phi) + \tilde{\mathcal{E}}_2 \cos 2(\beta-\phi)}{\tilde{\mathcal{E}}_5 \sin 2(\phi-\alpha) - \tilde{\mathcal{E}}_6 \cos 2(\phi-\alpha)}, \tag{40}$$

respectively. The relevant expressions for $\mathcal{E}_i$ and $\tilde{\mathcal{E}}_i$ are reported in Eqs. (A5) and (A10) of appendix. The correlation of neutrino masses m_1, m_2, and m_3 with the unknown parameter ϕ are shown in Figs. 11(a) and 12(a), respectively for TM_1 and TM_2 mixing matrix. It is observed that, it shows normal mass ordering for TM_1 mixing matrix, whereas, for TM_2 mixing matrix, it shows both normal and inverted mass ordering. The correlation of M_{ee} and $\sum m_i$ are shown in Figs. 11(b) and 12(b), respectively using TM_1 and TM_2 mixing matrix. In Figs. 11(c) and 12(c), we have shown the correlation of M_ν with $\sum m_i$ using TM_1 and TM_2 mixing matrix, respectively.

The allowed ranges of all the relevant parameters such as the absolute neutrino mass, the effective Majorana mass and the effective electron antineutrino mass under normal and inverted ordering for both the mixing matrix are reported in Table VII.

TABLE VII. Allowed range of $\sum m_i$, m_{ee}, and m_ν for C_{32} pattern.

Mixing matrix	Mass ordering	$\sum m_i$ (eV)	m_{ee} (eV)	m_ν (eV)
TM_1	**NO**	[0.061, 0.261]	$[1.309 \times 10^{-4}, 0.063$	[0.011, 0.082]
TM_2	**NO**	[0.056, 0.507]	$[6.054 \times 10^{-5}, 0.164]$	[0.084, 0.166]
	IO	[0.101, 0.346]	[0.017, 0.078]	[0.045, 0.118]

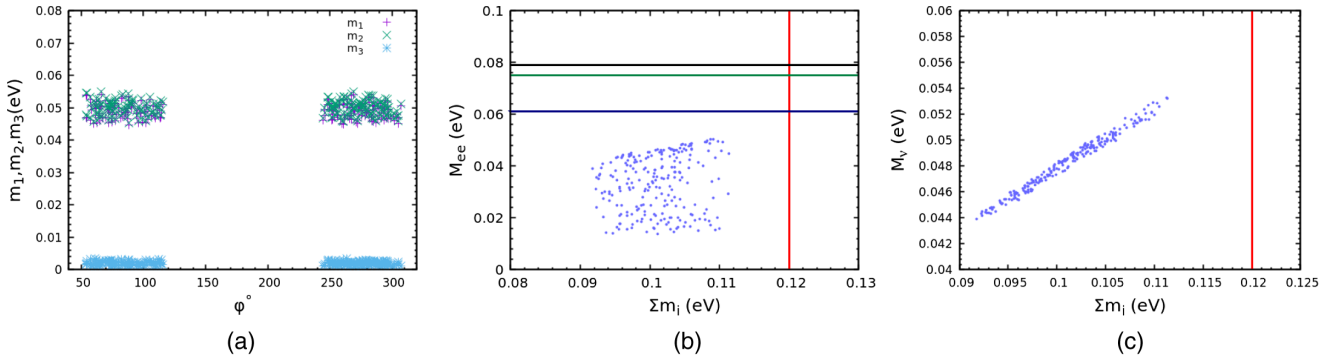

FIG. 13. (a) Variation of m_1, m_2, and m_3 as a function of ϕ, (b) correlation of $\sum m_i$ and m_{ee}, and (c) correlation of $\sum m_i$ and m_ν for C_{11} pattern using TM_1 mixing matrix. The vertical red line represents the upper bound of the total neutrino mass reported in Ref. [3]. The black, green, and blue lines represent the experimental upper bounds of the effective Majorana mass reported in Refs. [4–7].

F. Pattern VI: $C_{11} = 0$

The vanishing minor condition for this pattern is given by

$$(M_\nu)_{\mu\mu}(M_\nu)_{\tau\tau} - (M_\nu)_{\tau\mu}(M_\nu)_{\mu\tau} = 0. \tag{41}$$

The two neutrino mass ratios can be obtained using the elements from the neutrino mass matrix. For TM_1 mixing matrix, we have

$$\frac{m_1}{m_2} = \frac{2\sin 2\beta}{\cos^2\theta \sin 2(\alpha-\beta)}, \qquad \frac{m_3}{m_2} = -\frac{\tan^2\theta \sin 2\beta}{\sin 2\alpha}, \tag{42}$$

and for TM_2 mixing matrix, we have

$$\frac{m_1}{m_2} = \frac{2\cos^2\theta \sin 2\beta}{\sin 2(\alpha-\beta)}, \qquad \frac{m_3}{m_2} = -\frac{2\sin^2\theta \sin 2\beta}{\sin 2\alpha}. \tag{43}$$

Using Eq. (42), we obtain the mass relation for TM_1 mixing matrix as

$$m_1 \sin 2(\alpha-\beta) - 2m_2 \sin 2\beta + m_3 \sin 2\alpha = 0 \tag{44}$$

and using Eq. (43), we obtain the mass relation for TM_2 mixing matrix as

$$m_1 \sin 2(\alpha-\beta) - 2m_2 \sin 2\beta - m_3 \sin 2\alpha = 0. \tag{45}$$

This pattern gives a clear inverted mass ordering for both TM_1 and TM_2 mixing matrix. The correlation of the neutrino masses m_1, m_2 and m_3 for both the mixing patterns with the unknown parameter ϕ is shown in Figs. 13(a) and 14(a), respectively. The correlation of M_{ee} with $\sum m_i$ for TM_1 and TM_2 are shown in Figs. 13(b) and 14(b), respectively. In Figs. 13(c) and 14(c), we have shown the correlation of M_ν with $\sum m_i$ for TM_1 and TM_2 mixing matrix, respectively.

The allowed ranges of the absolute neutrino mass, the effective Majorana mass and the effective electron anti-neutrino mass obtained for both the mixing matrix are listed in the Table VIII.

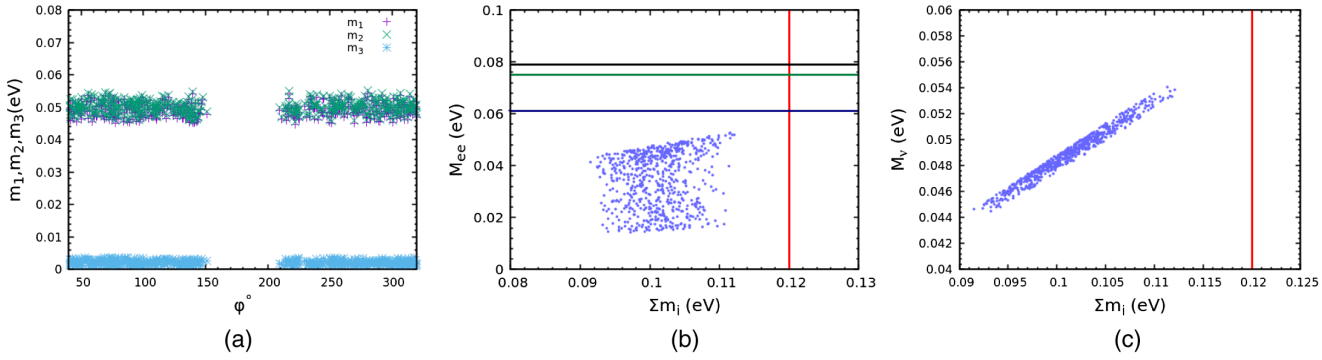

FIG. 14. (a) Variation of m_1, m_2, and m_3 as a function of ϕ, (b) correlation of $\sum m_i$ and m_{ee}, and (c) correlation of $\sum m_i$ and m_ν for C_{11} pattern using TM_2 mixing matrix. The vertical red line is the upper bound of the total neutrino mass reported in Ref. [3]. The black, green, and blue lines are the experimental upper bounds of the effective Majorana mass reported in Refs. [4–7].

TABLE VIII. Allowed range of $\sum m_i$, m_{ee}, and m_ν for C_{11} pattern.

Mixing matrix	Mass ordering	$\sum m_i$ (eV)	m_{ee} (eV)	m_ν (eV)
TM_1	**IO**	[0.092, 0.111]	[0.013, 0.050]	[0.043, 0.053]
TM_2	**IO**	[0.091, 0.112]	[0.014, 0.052]	[0.044, 0.054]

VI. DEGREE OF FINE TUNING IN THE NEUTRINO MASS MATRIX

In this section, we wish to determine whether the entries of the neutrino mass matrix are fine tuned or not. In order to determine the degree of fine tuning of the mass matrix elements, we define a parameter $d_{\rm FT}$ [19,56] which is obtained as the sum of the absolute values of the ratios between each parameter and its error. We follow Refs. [19,56] and define the fine tuning parameter as

$$d_{\rm FT} = \sum \left| \frac{{\rm par}_i}{{\rm err}_i} \right|, \tag{46}$$

where ${\rm par}_i = (\theta_{12}, \theta_{13}, \theta_{23}, \Delta m^2_{21}, \Delta m^2_{31})$ is the best fit values of the parameters. The error ${\rm err}_i$ for each parameter is obtained from the shift of best fit value that changes the $\chi^2_{\rm min}$ value by one unit keeping all other parameters fixed at their best fit values. To determine the best fit values of all the parameters, we perform a χ^2 analysis of all the classes of one minor zero and find the $\chi^2_{\rm min}$. We define the χ^2 as follows:

$$\chi^2 = \sum_{i=1}^{3} \frac{(\theta_i^{\rm cal} - \theta_i^{\rm exp})^2}{(\sigma_i^{\rm exp})^2} + \sum_{j=21,3l} \frac{(\Delta m_j^{\rm cal} - \Delta m_j^{\rm exp})^2}{(\sigma_j^{\rm exp})^2}, \tag{47}$$

where $\theta_i = (\theta_{12}, \theta_{13}, \theta_{23})$ and $\Delta m_j = (\Delta m^2_{21}, \Delta m^2_{31})$. Here $\theta_i^{\rm cal}$ and $\Delta m_j^{\rm cal}$ represent the theoretical value of θ_i and Δm_j, respectively, whereas $\theta_i^{\rm exp}$ and $\Delta m_j^{\rm exp}$ represent measured central value of θ_i and Δm_j, respectively. It should be noted that $\theta_i^{\rm cal}$ and $\Delta m_j^{\rm cal}$ depend on four unknown model parameters, namely θ, ϕ, α, and β. Similarly, the uncertainties in the measured value of θ_i and Δm_j are represented by $\sigma_i^{\rm exp}$ and $\sigma_j^{\rm exp}$, respectively. The central values and the corresponding uncertainties in each parameter are reported in Table II.

We first compute $d_{\rm Data}$ which is defined as the sum of the absolute values of the ratios between the measured values of each parameter and its error from Table II. We obtain the value of $d_{\rm Data}$ to be around 200 for both normal and inverted ordering case. The degree of fine tuning can be roughly estimated from the value of $d_{\rm FT}$ because if the $d_{\rm FT}$ value is large then a minimal variation of the corresponding parameters give large difference on the value of χ^2. Hence a large value of $d_{\rm FT}$ corresponds to a strong fine tuning of the mass matrix elements and vice versa. The $\chi^2_{\rm min}$ value and the corresponding best fit values of the unknown parameters of the neutrino mass matrix θ, ϕ, α, β and the value of d_{FT} parameter for each patterns are listed in the Tables IX and X for the TM_1 and TM_2 mixing matrix respectively. We also report the best fit values of several observables such as θ_{12}, θ_{13}, θ_{23}, Δm^2_{21}, and Δm^2_{31} for each pattern. For the patterns C_{33}, C_{22}, C_{31}, C_{32}, and C_{21}, the results are for NO case and for the pattern C_{11}, the results are for the IO case. As the pattern C_{11} follows the IO, the $\chi^2_{\rm min}$ value obtained for this pattern is large for both TM_1 and TM_2 mixing matrix. The best fit values of the mixing angles θ_{23}, θ_{12}, θ_{13} and the mass squared differences Δm^2_{21}, Δm^2_{31} obtained for each pattern are compatible with the experimentally measured values reported in Table II.

In case of TM_1 mixing matrix, pattern C_{23} shows very good agreement with the data with a very small $d_{\rm FT}$ value. Although, the pattern C_{31} also have same χ^2 as pattern C_{23}, it, however, has a much larger $d_{\rm FT}$ value compared to pattern C_{23}. It can be concluded that for the pattern C_{31}, there is a strong fine tuning among the elements of the mass

TABLE IX. The values of $\chi^2_{\rm min}$, $d_{\rm FT}$, the best fit values of θ°_{13}, θ°_{12}, θ°_{23}, θ°, ϕ°, α°, β°, $\Delta m^2_{21}(10^{-5}\ {\rm eV}^2)$, and $\Delta m^2_{3l}(10^{-3}\ {\rm eV}^2)$ for TM_1 mixing matrix.

Type	$\chi^2_{\rm min}$	$d_{\rm FT}$	θ°_{13}	θ°_{12}	θ°_{23}	θ°	ϕ°	α°	β°	Δm^2_{21} $(10^{-5}\ {\rm eV}^2)$	Δm^2_{3l} $(10^{-3}\ {\rm eV}^2)$
C_{33}	2.66	8.38×10^3	8.48	34.35	48.59	14.80	287.67	290.89	320.72	7.51	2.42
C_{22}	2.80	2.35×10^5	8.46	34.36	48.77	14.77	251.38	313.24	74.37	7.48	2.45
C_{31}	1.69	8.43×10^3	8.57	34.33	48.83	14.96	108.69	7.46	338.00	7.47	2.44
C_{32}	1.69	83.72	8.60	34.33	49.56	15.02	76.68	84.95	357.14	7.47	2.44
C_{21}	3.24	1.36×10^5	8.67	34.31	50.00	15.07	63.50	269.82	216.81	7.47	2.41
C_{11}	4.05	4.88×10^2	8.41	34.37	49.33	14.68	291.60	188.42	83.27	7.40	−2.46

TABLE X. The values of $\chi^2_{\min}$, $d_{\rm FT}$, the best fit values of θ°_{13}, θ°_{12}, θ°_{23}, θ°, ϕ°, α°, β°, $\Delta m^2_{21}(10^{-5}\ \mathrm{eV}^2)$, and $\Delta m^2_{3l}(10^{-3}\ \mathrm{eV}^2)$ for TM_2 mixing matrix.

Type	$\chi^2_{\min}$	$d_{\rm FT}$	θ°_{13}	θ°_{12}	θ°_{23}	θ°	ϕ°	α°	β°	$\Delta m^2_{21}(10^{-5}\ \mathrm{eV}^2)$	$\Delta m^2_{3l}\,(10^{-3}\ \mathrm{eV}^2)$
C_{33}	8.87	5.86×10^2	8.57	35.72	48.95	10.52	310.43	178.66	169.70	7.42	2.43
C_{22}	9.08	4.31×10^2	8.59	35.72	48.85	10.54	230.78	63.70	184.68	7.37	4.43
C_{31}	9.23	4.78×10^4	8.55	35.72	48.50	10.49	234.75	185.56	217.34	7.37	2.44
C_{32}	9.29	1.09×10^2	8.56	35.72	48.94	10.51	310.43	355.65	82.48	7.50	2.44
C_{21}	9.12	2.07×10^3	8.54	35.70	49.80	10.47	142.15	279.77	59.23	7.40	2.43
C_{11}	9.82	2.29×10^2	8.65	35.73	50.55	10.62	25.81	341.08	103.82	7.42	−2.49

matrix. Similarly, C_{22}, C_{21}, and C_{33} have larger $d_{\rm FT}$ value compared to C_{11} pattern, although they have less χ^2 value than C_{11}. For C_{22}, C_{21}, and C_{33} also the degree of fine tuning among the mass matrix elements is very strong. Moreover, it is very clear from Table IX that all these patterns prefer the atmospheric mixing angle θ_{23} to be greater than $\pi/4$. Based on the $d_{\rm FT}$ values, it is clear that it requires less fine tuning of the mass matrix elements for patterns C_{23} and C_{11}.

For the TM_2 mixing matrix, the fine-tuned parameter $d_{\rm FT}$ is small for the patterns C_{33}, C_{22}, C_{32}, and C_{11}. Among all these patterns C_{32} has the lowest $d_{\rm FT}$ value. However, for patterns C_{31} and C_{21}, $d_{\rm FT}$ value is quite large and hence the degree of fine tuning among the elements of the mass matrix is quite strong for these patterns. All the patterns prefer the best fit value of θ_{23} to be larger than $\pi/4$.

VII. SYMMETRY REALIZATION

The symmetry of one vanishing minor can be realized through type-I seesaw mechanism [57,58] along with Abelian symmetry. One vanishing minor in the neutrino mass matrix can easily be obtained if one element in the Majorana matrix M_R is zero along with diagonal Dirac mass matrix M_D. In order to fulfill this condition, we need three right-handed charged lepton l_{Rp} ($p=1,2,3$), three right-handed neutrinos ν_{Rp} and three left-handed lepton doublets D_{Lp}. We present the symmetry realization of pattern V. The symmetry of this pattern can be realized through the Abelian symmetry group $(Z_{12}\times Z_2)$ that is discussed in Refs. [27,59].

The leptonic fields under Z_{12} transform as

$$\begin{aligned}
&\bar{l}_{R1}\to\omega\bar{l}_{R1}, \quad \bar{\nu}_{R1}\to\omega\bar{\nu}_{R1}, \quad D_{L1}\to\omega\bar{D}_{L1},\\
&\bar{l}_{R2}\to\omega^2\bar{l}_{R2}, \quad \bar{\nu}_{R2}\to\omega^2\bar{\nu}_{R2}, \quad D_{L2}\to\omega^3\bar{D}_{L2},\\
&\bar{l}_{R3}\to\omega^5\bar{l}_{R3}, \quad \bar{\nu}_{R3}\to\omega^5\bar{\nu}_{R3}, \quad D_{L3}\to\omega^8\bar{D}_{L3},
\end{aligned} \tag{48}$$

where $\omega=\exp(\frac{i\pi}{6})$. The bilinears $\bar{l}_{Rp}D_{Lq}$ and $\bar{\nu}_{Rp}D_{Lq}$, where $p,\ q=1,\ 2,\ 3$, relevant for $(M_l)_{pq}$ and $(M_D)_{pq}$ transform as $\bar{l}_{Rp}D_{Lq}\to\Omega l_{Rp}D_{Lq}$, where

$$\Omega=\begin{pmatrix}\omega^2 & \omega^4 & \omega^9\\ \omega^3 & \omega^5 & \omega^{10}\\ \omega^6 & \omega^8 & \omega\end{pmatrix} \tag{49}$$

and the bilinears $\bar{\nu}_{Rp}C\bar{\nu}^T_{Rq}$ relevant for $(M_R)_{pq}$ transform as $\bar{\nu}_{Rp}C\bar{\nu}^T_{Rq}\to\Lambda\bar{\nu}_{Rp}C\bar{\nu}^T_{Rq}$, where

$$\Lambda=\begin{pmatrix}\omega^2 & \omega^3 & \omega^6\\ \omega^3 & \omega^4 & \omega^7\\ \omega^6 & \omega^7 & \omega^{10}\end{pmatrix}. \tag{50}$$

For each nonzero element in M_R, we need a scalar singlet χ_{pq} and for each nonzero element in $(M_l)_{pq}$ or $(M_D)_{pq}$, we need Higgs scalar ϕ_{pq} or $\tilde{\phi}_{pq}$, respectively. The scalar singlets get the vacuum expectation values (vevs) at the seesaw scale, while Higgs doublets get vevs at the electroweak scale. Under Z_2 transformation, the sign of $\tilde{\phi}_{pq}$ and ν_{Rp} changes, while other multiplets remain invariant. The diagonal charged lepton mass matrix can be obtained by introducing only three Higgs doublets namely ϕ_{11}, ϕ_{22}, and ϕ_{33}, similarly, the diagonal Dirac neutrino mass matrix can be obtained by introducing three Higgs doublets $\tilde{\phi}_{11}$, $\tilde{\phi}_{22}$, and $\tilde{\phi}_{33}$. The nonzero elements of M_R can be obtained by introducing scalar fields χ_{11}, χ_{12}, χ_{13}, χ_{22}, and χ_{33} which under Z_{12} transformation gets multiplied by ω^{10}, ω^9, ω^6, ω^8, and ω^2, respectively. The Majorana mass matrix M_R can be written as

$$M_R=\begin{pmatrix}a & b & c\\ b & d & 0\\ c & 0 & e\end{pmatrix}. \tag{51}$$

This provides minor zero corresponding to (3,2) element in the neutrino mass matrix. Other patterns can also be realized similarly for different M_R.

VIII. CONCLUSION

We explore the implication of one minor zero in the neutrino mass matrix obtained using trimaximal mixing matrix. There are total six possible patterns and all the patterns are found to be phenomenologically compatible with the present neutrino oscillation data. The two unknown parameters θ and ϕ of the trimaximal mixing matrix are determined by using the experimental values of the mixing angles θ_{12}, θ_{23}, and θ_{13}. It is found that TM_1 mixing matrix provides a better fit to the experimental results than TM_2 mixing matrix. The Jarlskog invariant measure of CP violation is nonzero for all the pattern, so they are necessarily CP violating. Patterns I, II, and V show normal mass ordering for TM_1 mixing matrix while these patterns show both normal and inverted mass ordering for TM_2 mixing matrix. Patterns III and IV show both normal and inverted mass ordering for both TM_1 and TM_2 mixing matrix. Pattern VI predicts inverted mass ordering for both the mixing matrix. We predict the unknown parameters such as the absolute neutrino mass scale, the effective Majorana mass and the effective electron antineutrino mass using both TM_1 and TM_2 mixing matrix. The effective Majorana mass obtained for each pattern is within the reach of neutrinoless double beta decay experiment. Similarly, the value obtained for the effective electron antineutrino mass may be within the reach of future Project 8 experiment. We also discuss the fine tuning of the elements of the mass matrix for all the patterns by introducing a new parameter d_{FT}. We observe that for the pattern C_{23}, the fine tuning among the elements of the mass matrix is small compared to other patterns. Moreover, we also discuss the symmetry realization of pattern V using Abelian symmetry group $Z_{12} \times Z_2$ in the framework of type-I seesaw model which can be easily generalized to all the other patterns as well.

APPENDIX

The coefficients in the mass ratios for the TM_1 mixing matrix can be expressed in terms of the two unknown parameters θ and ϕ as

$$\mathcal{A}_1 = \frac{1}{6}\left(\frac{1}{3}\sin^2\theta + \frac{1}{2}\cos^2\theta\cos 2\phi - \sqrt{\frac{2}{3}}\sin\theta\cos\theta\cos\phi\right),$$

$$\mathcal{A}_2 = \frac{1}{6}\left(\frac{1}{2}\cos^2\theta\sin 2\phi - \sqrt{\frac{2}{3}}\sin\theta\cos\theta\sin\phi\right),$$

$$\mathcal{A}_3 = \left(\frac{1}{3}\cos^2\theta + \frac{1}{2}\sin^2\theta\cos 2\phi + \sqrt{\frac{2}{3}}\sin\theta\cos\theta\cos\phi\right)\left(\frac{1}{3}\sin^2\theta + \frac{1}{2}\cos^2\theta\cos 2\phi - \sqrt{\frac{2}{3}}\sin\theta\cos\theta\cos\phi\right),$$

$$\mathcal{A}_4 = \left(\frac{1}{2}\sin^2\theta\sin 2\phi + \sqrt{\frac{2}{3}}\sin\theta\cos\theta\sin\phi\right)\left(\frac{1}{2}\cos^2\theta\sin 2\phi - \sqrt{\frac{2}{3}}\sin\theta\cos\theta\cos\phi\right),$$

$$\mathcal{A}_5 = \left(\frac{1}{2}\sin^2\theta\sin 2\phi + \sqrt{\frac{2}{3}}\sin\theta\cos\theta\sin\phi\right)\left(\frac{1}{3}\sin^2\theta + \frac{1}{2}\cos^2\theta\cos 2\phi - \sqrt{\frac{2}{3}}\sin\theta\cos\theta\cos\phi\right),$$

$$\mathcal{A}_6 = \left(\frac{1}{3}\cos^2\theta + \frac{1}{2}\sin^2\theta\cos 2\phi + \sqrt{\frac{2}{3}}\sin\theta\cos\theta\cos\phi\right)\left(\frac{1}{2}\cos^2\theta\sin 2\phi - \sqrt{\frac{2}{3}}\sin\theta\cos\theta\sin\phi\right),$$

$$\mathcal{A}_7 = -\frac{1}{6}\left(\frac{1}{3}\cos^2\theta + \frac{1}{2}\sin^2\theta\cos 2\phi + \sqrt{\frac{2}{3}}\sin\theta\cos\theta\cos\phi\right),$$

$$\mathcal{A}_8 = -\frac{1}{6}\left(\frac{1}{2}\sin^2\theta\sin 2\phi + \sqrt{\frac{2}{3}}\sin\theta\cos\theta\sin\phi\right). \tag{A1}$$

$$\mathcal{B}_1 = \frac{1}{6}\left(\frac{1}{3}\sin^2\theta + \frac{1}{2}\cos^2\theta\cos 2\phi + \sqrt{\frac{2}{3}}\sin\theta\cos\theta\cos\phi\right),$$
$$\mathcal{B}_2 = \frac{1}{6}\left(\frac{1}{2}\cos^2\theta\sin 2\phi + \sqrt{\frac{2}{3}}\sin\theta\cos\theta\sin\phi\right),$$
$$\mathcal{B}_3 = \left(\frac{1}{3}\cos^2\theta + \frac{1}{2}\sin^2\theta\cos 2\phi - \sqrt{\frac{2}{3}}\sin\theta\cos\theta\cos\phi\right)\left(\frac{1}{3}\sin^2\theta + \frac{1}{2}\cos^2\theta\cos 2\phi + \sqrt{\frac{2}{3}}\sin\theta\cos\theta\cos\phi\right),$$
$$\mathcal{B}_4 = \left(\frac{1}{2}\sin^2\theta\sin 2\phi - \sqrt{\frac{2}{3}}\sin\theta\cos\theta\sin\phi\right)\left(\frac{1}{2}\cos^2\theta\sin 2\phi + \sqrt{\frac{2}{3}}\sin\theta\cos\theta\cos\phi\right),$$
$$\mathcal{B}_5 = \left(\frac{1}{2}\cos^2\theta\sin 2\phi + \sqrt{\frac{2}{3}}\sin\theta\cos\theta\sin\phi\right)\left(\frac{1}{3}\cos^2\theta + \frac{1}{2}\sin^2\theta\cos 2\phi - \sqrt{\frac{2}{3}}\sin\theta\cos\theta\cos\phi\right),$$
$$\mathcal{B}_6 = \left(\frac{1}{3}\sin^2\theta + \frac{1}{2}\cos^2\theta\cos 2\phi + \sqrt{\frac{2}{3}}\sin\theta\cos\theta\cos\phi\right)\left(\frac{1}{2}\sin^2\theta\sin 2\phi - \sqrt{\frac{2}{3}}\sin\theta\cos\theta\sin\phi\right),$$
$$\mathcal{B}_7 = -\frac{1}{6}\left(\frac{1}{3}\cos^2\theta + \frac{1}{2}\sin^2\theta\cos 2\phi - \sqrt{\frac{2}{3}}\sin\theta\cos\theta\cos\phi\right),$$
$$\mathcal{B}_8 = -\frac{1}{6}\left(\frac{1}{2}\sin^2\theta\sin 2\phi - \sqrt{\frac{2}{3}}\sin\theta\cos\theta\sin\phi\right). \tag{A2}$$

$$\mathcal{C}_1 = -\frac{1}{3}\left(\frac{1}{3}\sin\theta\cos\theta - \sqrt{\frac{1}{6}}\cos^2\theta\cos\phi\right),$$
$$\mathcal{C}_2 = -\frac{1}{3\sqrt{6}}(\cos^2\theta\sin\phi),$$
$$\mathcal{C}_3 = \left(\frac{1}{6}\sin\theta\cos^3\theta\sin^2\phi\right) - \left(\frac{1}{3}\cos^2\theta + \sqrt{\frac{1}{6}}\sin\theta\cos\theta\sin\phi\right)\left(\frac{1}{3}\sin\theta\cos\theta - \sqrt{\frac{1}{6}}\cos^2\theta\cos\phi\right),$$
$$\mathcal{C}_4 = \sqrt{\frac{1}{6}}\cos^2\theta\sin\phi\left(\frac{1}{3}\cos^2\theta + \sqrt{\frac{1}{6}}\sin\theta\cos\theta\cos\phi\right) + \sqrt{\frac{1}{6}}\sin\theta\cos\theta\cos\phi\left(\frac{1}{3}\sin\theta\cos\theta - \sqrt{\frac{1}{6}}\cos^2\theta\cos\phi\right),$$
$$\mathcal{C}_5 = \frac{1}{3}\left(\frac{1}{3}\cos^2\theta + \sqrt{\frac{1}{6}}\sin\theta\cos\theta\cos\phi\right),$$
$$\mathcal{C}_6 = \frac{1}{3\sqrt{6}}\sin\theta\cos\theta\sin\phi. \tag{A3}$$

$$\mathcal{D}_1 = -\frac{1}{3}\left(\frac{1}{3}\sin^2\theta - \sqrt{\frac{1}{6}}\sin\theta\cos\theta\cos\phi\right),$$
$$\mathcal{D}_2 = -\frac{1}{3\sqrt{6}}(\cos\theta\sin\phi),$$
$$\mathcal{D}_3 = \left(\frac{1}{6}\sin^2\theta\cos^2\theta\sin^2\phi\right) + \left(\frac{1}{3}\cos^2\theta - \sqrt{\frac{1}{6}}\sin\theta\cos\theta\cos\phi\right)\left(\frac{1}{3}\sin^2\theta - \sqrt{\frac{1}{6}}\sin\theta\cos\theta\cos\phi\right),$$
$$\mathcal{D}_4 = \sqrt{\frac{1}{6}}\sin\theta\cos\theta\sin\phi\left(\frac{1}{3}\sin^2\theta + \sqrt{\frac{1}{6}}\sin\theta\cos\theta\cos\phi\right) - \sqrt{\frac{1}{6}}\sin\theta\cos\theta\sin\phi\left(\frac{1}{3}\cos^2\theta - \sqrt{\frac{1}{6}}\sin\theta\cos\theta\cos\phi\right),$$
$$\mathcal{D}_5 = \frac{1}{3}\left(\frac{1}{3}\cos^2\theta - \sqrt{\frac{1}{6}}\sin\theta\cos\theta\cos\phi\right),$$
$$\mathcal{D}_6 = \frac{1}{3\sqrt{6}}\sin\theta\cos\theta\sin\phi. \tag{A4}$$

$$\mathcal{E}_1 = -\frac{1}{6}\left(\frac{1}{2}\cos^2\theta \sin 2\phi - \frac{1}{2}\sin^2\theta\right),$$
$$\mathcal{E}_2 = -\frac{1}{12}(\cos^2\theta \sin 2\phi),$$
$$\mathcal{E}_3 = \left(\frac{1}{4}\sin^2\theta\cos^2\theta\sin^2 2\phi\right) - \left(\frac{1}{3}\cos^2\theta - \frac{1}{2}\sin^2\theta\cos 2\phi\right)\left(\frac{1}{2}\cos^2\theta\cos 2\phi - \frac{1}{3}\sin^2\theta\right),$$
$$\mathcal{E}_4 = \frac{1}{2}\cos^2\theta \sin 2\phi\left(\frac{1}{3}\cos^2\theta - \frac{1}{2}\sin^2\theta\cos 2\phi\right) + \frac{1}{2}\sin^2\theta \sin 2\phi\left(\frac{1}{2}\cos^2\theta\cos 2\phi - \frac{1}{3}\sin^2\theta\right),$$
$$\mathcal{E}_5 = -\frac{1}{6}\left(\frac{1}{3}\cos^2\theta - \frac{1}{2}\sin^2\theta\cos 2\phi\right),$$
$$\mathcal{E}_6 = \frac{1}{12}\sin^2\theta \sin 2\phi. \tag{A5}$$

Similarly, the coefficients in the mass ratios for the TM_2 mixing can be written as

$$\tilde{\mathcal{A}}_1 = \frac{10}{36}\sin^2\theta\cos^2\theta\cos 2\phi + \frac{1}{12}\sin^4\theta - \frac{1}{6\sqrt{3}}\sin^2\theta \sin 2\theta\cos\phi + \frac{1}{12}\cos^4\theta(\cos^2 2\phi - \sin^2 2\phi),$$
$$\tilde{\mathcal{A}}_2 = \frac{1}{6\sqrt{3}}\cos^2\theta \sin 2\theta\cos 3\phi - \frac{1}{12}\sin^2 2\theta\cos 2\phi,$$
$$\tilde{\mathcal{A}}_3 = \frac{10}{36}\sin^2\theta\cos^2\theta \sin 2\phi - \frac{1}{6\sqrt{3}}\sin^2\theta \sin 2\theta\sin\phi + \frac{1}{6}\cos^4\theta\cos 2\phi \sin 2\phi,$$
$$\tilde{\mathcal{A}}_4 = \frac{1}{6\sqrt{3}}\cos^2\theta \sin 2\theta\sin 3\phi - \frac{1}{12}\sin^2 2\theta \sin 2\phi,$$
$$\tilde{\mathcal{A}}_5 = \frac{1}{18}\sin^2\theta + \frac{1}{6}\cos^2\theta\cos 2\phi - \frac{1}{6\sqrt{3}}\sin 2\theta\cos\phi,$$
$$\tilde{\mathcal{A}}_6 = \frac{1}{6}\cos^2\theta \sin 2\phi - \frac{1}{6\sqrt{3}}\sin 2\theta\sin\phi,$$
$$\tilde{\mathcal{A}}_7 = \frac{1}{6}\sin^2\theta + \frac{1}{18}\cos^2\theta\cos 2\phi + \frac{1}{6\sqrt{3}}\sin 2\theta\cos\phi,$$
$$\tilde{\mathcal{A}}_8 = \frac{1}{18}\cos^2\theta \sin 2\phi + \frac{1}{6\sqrt{3}}\sin 2\theta\sin\phi. \tag{A6}$$

$$\tilde{\mathcal{B}}_1 = \frac{10}{36}\sin^2\theta\cos^2\theta\cos 2\phi + \frac{1}{12}\sin^4\theta + \frac{1}{6\sqrt{3}}\sin^2\theta \sin 2\theta\cos\phi + \frac{1}{12}\cos^4\theta(\cos^2 2\phi - \sin^2 2\phi),$$
$$\tilde{\mathcal{B}}_2 = -\frac{1}{6\sqrt{3}}\cos^2\theta \sin 2\theta\cos 3\phi - \frac{1}{12}\sin^2 2\theta\cos 2\phi,$$
$$\tilde{\mathcal{B}}_3 = \frac{10}{36}\sin^2\theta\cos^2\theta \sin 2\phi + \frac{1}{6\sqrt{3}}\sin^2\theta \sin 2\theta\sin\phi + \frac{1}{6}\cos^4\theta\cos 2\phi \sin 2\phi,$$
$$\tilde{\mathcal{B}}_4 = -\frac{1}{6\sqrt{3}}\cos^2\theta \sin 2\theta\sin 3\phi - \frac{1}{12}\sin^2 2\theta \sin 2\phi,$$
$$\tilde{\mathcal{B}}_5 = \frac{1}{18}\sin^2\theta + \frac{1}{6}\cos^2\theta\cos 2\phi + \frac{1}{6\sqrt{3}}\sin 2\theta\sin\phi,$$
$$\tilde{\mathcal{B}}_6 = \frac{1}{6}\cos^2\theta \sin 2\phi + \frac{1}{6\sqrt{3}}\sin 2\theta\sin\phi,$$
$$\tilde{\mathcal{B}}_7 = \frac{1}{6}\sin^2\theta + \frac{1}{18}\cos^2\theta\cos 2\phi - \frac{1}{6\sqrt{3}}\sin 2\theta\cos\phi,$$
$$\tilde{\mathcal{B}}_8 = \frac{1}{18}\cos^2\theta \sin 2\phi - \frac{1}{6\sqrt{3}}\sin 2\theta\sin\phi. \tag{A7}$$

$$\tilde{\mathcal{C}}_1 = \frac{1}{9}\sin^2\theta\cos^2\theta\cos 2\phi - \frac{1}{6\sqrt{3}}\cos^2\theta\sin 2\theta\cos 3\phi + \frac{1}{6\sqrt{3}}\sin^2\theta\sin 2\theta\cos\phi - \frac{1}{12}\sin^2 2\theta\cos 2\phi,$$
$$\tilde{\mathcal{C}}_2 = \frac{1}{9}\sin^2\theta\cos^2\theta\sin 2\phi - \frac{1}{6\sqrt{3}}\cos^2\theta\sin 2\theta\sin 3\phi + \frac{1}{6\sqrt{3}}\sin^2\theta\sin 2\theta\sin\phi - \frac{1}{12}\sin^2\theta\sin 2\phi,$$
$$\tilde{\mathcal{C}}_3 = \frac{1}{6\sqrt{3}}\sin 2\theta\cos\phi - \frac{1}{9}\sin^2\theta,$$
$$\tilde{\mathcal{C}}_4 = \frac{1}{6\sqrt{3}}\sin 2\theta\sin\phi,$$
$$\tilde{\mathcal{C}}_5 = \frac{1}{9}\cos^2\theta\cos 2\phi + \frac{1}{6\sqrt{3}}\sin 2\theta\cos\phi,$$
$$\tilde{\mathcal{C}}_6 = \frac{1}{9}\cos^2\theta\sin 2\phi + \frac{1}{6\sqrt{3}}\sin 2\theta\sin\phi. \tag{A8}$$

$$\tilde{\mathcal{D}}_1 = \frac{1}{9}\sin^2\theta\cos^2\theta\cos 2\phi - \frac{1}{6\sqrt{3}}\sin^2\theta\sin 2\theta\cos 3\phi + \frac{1}{6\sqrt{3}}\cos^2\theta\sin 2\theta\cos\phi - \frac{1}{12}\sin^2 2\theta\cos 2\phi,$$
$$\tilde{\mathcal{D}}_2 = \frac{1}{9}\sin^2\theta\cos^2\theta\sin 2\phi - \frac{1}{6\sqrt{3}}\sin^2\theta\sin 2\theta\sin\phi + \frac{1}{6\sqrt{3}}\cos^2\theta\sin 2\theta\sin 3\phi - \frac{1}{12}\sin^2\theta\sin 2\phi,$$
$$\tilde{\mathcal{D}}_3 = \frac{1}{6\sqrt{3}}\sin 2\theta\cos\phi + \frac{1}{9}\sin^2\theta,$$
$$\tilde{\mathcal{D}}_4 = \frac{1}{6\sqrt{3}}\sin 2\theta\sin\phi,$$
$$\tilde{\mathcal{D}}_5 = \frac{1}{9}\cos^2\theta\cos 2\phi - \frac{1}{6\sqrt{3}}\sin 2\theta\cos\phi,$$
$$\tilde{\mathcal{D}}_6 = \frac{1}{6\sqrt{3}}\sin 2\theta\sin\phi - \frac{1}{9}\cos^2\theta\sin 2\phi. \tag{A9}$$

$$\tilde{\mathcal{E}}_1 = \frac{10}{36}\sin^2\theta\cos^2\theta\cos 2\phi - \frac{1}{12}\cos^4\theta\cos^2 2\phi - \frac{1}{12}\sin^4\theta + \frac{1}{12}\cos^4\theta\sin^2 2\phi,$$
$$\tilde{\mathcal{E}}_2 = \frac{5}{18}\sin^2\theta\cos^2\theta\sin 2\phi - \frac{1}{6}\cos^4\theta\sin 2\phi\cos 2\phi,$$
$$\tilde{\mathcal{E}}_3 = \frac{1}{6}\cos^2\theta\cos 2\phi - \frac{1}{18}\sin^2\theta,$$
$$\tilde{\mathcal{E}}_4 = \frac{1}{6}\cos^2\theta\sin 2\phi,$$
$$\tilde{\mathcal{E}}_5 = \frac{1}{6}\sin^2\theta - \frac{1}{18}\cos^2\theta\cos 2\phi,$$
$$\tilde{\mathcal{E}}_6 = \frac{1}{6}\cos^2\theta\sin 2\phi. \tag{A10}$$

[1] Y. Fukuda *et al.* (Super-Kamiokande Collaboration), Phys. Rev. Lett. **81**, 1562 (1998).
[2] A. A. Esfahani *et al.* (Project 8 Collaboration), arXiv:2203.07349.
[3] M. Zhang, J. F. Zhang, and X. Zhang, Commun. Theor. Phys. **72**, 125402 (2020).
[4] M. Agostini *et al.* (GERDA Collaboration), Phys. Rev. Lett. **111**, 122503 (2013).
[5] K. Alfonso *et al.* (CUORE Collaboration), Phys. Rev. Lett. **115**, 102502 (2015).
[6] J. B. Albert *et al.* (EXO-200 Collaboration), Nature (London) **510**, 229 (2014).
[7] A. Gando *et al.* (KamLAND-Zen Collaboration), Phys. Rev. Lett. **110**, 062502 (2013).
[8] E. I. Lashin and N. Chamoun, Phys. Rev. D **85**, 113011 (2012).
[9] M. Singh, Adv. High Energy Phys. **2018**, 2863184 (2018).
[10] R. R. Gautam, Phys. Rev. D **97**, 055022 (2018).
[11] P. H. Frampton, S. L. Glashow, and D. Marfatia, Phys. Lett. B **536**, 79 (2002).
[12] Z. z. Xing, Phys. Lett. B **530**, 159 (2002).
[13] Z. z. Xing, Phys. Lett. B **539**, 85 (2002).
[14] L. Lavoura, Phys. Lett. B **609**, 317 (2005).
[15] S. Dev, S. Kumar, S. Verma, and S. Gupta, Phys. Rev. D **76**, 013002 (2007).
[16] S. Kumar, Phys. Rev. D **84**, 077301 (2011).
[17] H. Fritzsch, Z. z. Xing, and S. Zhou, J. High Energy Phys. 09 (2011) 083.
[18] P. O. Ludl, S. Morisi, and E. Peinado, Nucl. Phys. **B857**, 411 (2012).
[19] D. Meloni and G. Blankenburg, Nucl. Phys. **B867**, 749 (2013).
[20] W. Grimus and P. O. Ludl, J. Phys. G **40**, 055003 (2013).
[21] S. Dev, R. R. Gautam, L. Singh, and M. Gupta, Phys. Rev. D **90**, 013021 (2014).
[22] R. R. Gautam and S. Kumar, Phys. Rev. D **94**, 036004 (2016); **100**, 039902(E) (2019).
[23] K. S. Channey and S. Kumar, J. Phys. G **46**, 015001 (2019).
[24] M. Singh, Europhys. Lett. **129**, 1 (2020).
[25] E. I. Lashin and N. Chamoun, Phys. Rev. D **78**, 073002 (2008).
[26] E. I. Lashin and N. Chamoun, Phys. Rev. D **80**, 093004 (2009).
[27] S. Dev, S. Verma, S. Gupta, and R. R. Gautam, Phys. Rev. D **81**, 053010 (2010).
[28] S. Dev, S. Gupta, and R. R. Gautam, Mod. Phys. Lett. A **26**, 501 (2011).
[29] Z. Tavartkiladze, Phys. Rev. D **106**, 115002 (2022).
[30] T. Araki, J. Heeck, and J. Kubo, J. High Energy Phys. 07 (2012) 083.
[31] J. Liao, D. Marfatia, and K. Whisnant, J. High Energy Phys. 09 (2014) 013.
[32] S. Dev, R. R. Gautam, and L. Singh, Phys. Rev. D **87**, 073011 (2013).
[33] W. Wang, Eur. Phys. J. C **73**, 2551 (2013).
[34] K. Whisnant, J. Liao, and D. Marfatia, AIP Conf. Proc. **1604**, 273 (2015).
[35] S. Dev, L. Singh, and D. Raj, Eur. Phys. J. C **75**, 394 (2015).
[36] W. Wang, S. Y. Guo, and Z. G. Wang, Mod. Phys. Lett. A **31**, 1650080 (2016).
[37] S. Goswami, S. Khan, and A. Watanabe, Phys. Lett. B **693**, 249 (2010).
[38] S. Dev, S. Verma, and S. Gupta, Phys. Lett. B **687**, 53 (2010).
[39] S. Dev, S. Gupta, and R. R. Gautam, Phys. Rev. D **82**, 073015 (2010).
[40] J. Y. Liu and S. Zhou, Phys. Rev. D **87**, 093010 (2013).
[41] S. Dev, R. R. Gautam, and L. Singh, Phys. Rev. D **88**, 033008 (2013).
[42] P. F. Harrison, D. H. Perkins, and W. G. Scott, Phys. Lett. B **530**, 167 (2002).
[43] P. F. Harrison and W. G. Scott, Phys. Lett. B **535**, 163 (2002).
[44] Z. z. Xing, Phys. Lett. B **533**, 85 (2002).
[45] P. F. Harrison and W. G. Scott, Phys. Lett. B **557**, 76 (2003).
[46] K. Abe *et al.* (T2K Collaboration), Phys. Rev. Lett. **107**, 041801 (2011).
[47] P. Adamson *et al.* (MINOS Collaboration), Phys. Rev. Lett. **107**, 181802 (2011).
[48] Y. Abe *et al.* (Double Chooz Collaboration), Phys. Rev. Lett. **108**, 131801 (2012).
[49] F. P. An *et al.* (Daya Bay Collaboration), Phys. Rev. Lett. **108**, 171803 (2012).
[50] J. K. Ahn *et al.* (RENO Collaboration), Phys. Rev. Lett. **108**, 191802 (2012).
[51] S. Kumar, Phys. Rev. D **82**, 013010 (2010); **85**, 079904(E) (2012).
[52] X. G. He and A. Zee, Phys. Rev. D **84**, 053004 (2011).
[53] W. Grimus and L. Lavoura, J. High Energy Phys. 09 (2008) 106.
[54] C. Jarlskog, Phys. Rev. Lett. **55**, 1039 (1985).
[55] I. Esteban, M. C. Gonzalez-Garcia, M. Maltoni, T. Schwetz, and A. Zhou, J. High Energy Phys. 09 (2020) 178.
[56] G. Altarelli and G. Blankenburg, J. High Energy Phys. 03 (2011) 133.
[57] P. Minkowski, Phys. Lett. **67B**, 421 (1977).
[58] R. N. Mohapatra and G. Senjanovic, Phys. Rev. Lett. **44**, 912 (1980).
[59] W. Grimus, A. S. Joshipura, L. Lavoura, and M. Tanimoto, Eur. Phys. J. C **36**, 227 (2004).